Environmental Impact, Mechanical Properties, and Productivity: Considerations on Filler Wire and Scanning Strategy in Laser Welding

(Article begins on next page)

12 September 2024

Environmental impact, mechanical properties and productivity: considerations on filler wire and scanning strategy in laser welding

Erica Liverani[a,b], Caterina Angeloni[a], Alessandro Ascari[a], Alessandro Fortunato[a]

(a) Department of Industrial Engineering (DIN), viale Risorgimento 2, Alma Mater Studiorum - University of Bologna, Bologna (Italy)
(b) Corresponding author: erica.liverani2@unibo.it., https://orcid.org/0000-0002-0010-6871, viale Risorgimento 2, 40136 Bologna, BO, Italy

ABSTRACT

Sustainability, as well as high-quality outcomes, pose significant challenges within the context of current manufacturing cycles, in alignment with European strategies aimed at decarbonization. This framework encourages a systematic evaluation of manufacturing processes in terms of their performance and carbon footprint. One sector where this is particularly relevant is the production of batteries for electric mobility, thanks to its exponential growth. Out of all the processes involved, laser welding stands out as being a critical step since it offers potential energy savings through optimization. With the dual goals of achieving mechanical strength and environmental sustainability, this study investigates alternative solutions for laser welding of aluminium sheets.

Different laser welding configurations are tested to evaluate the effect of process setups on weld quality and carbon emissions across different productivity scenarios.

The key findings can be summarized as follows: (1) the selection of welding setup significantly influences both quality and sustainability requirements; (2) the optimal conditions for meeting strength requirements may diverge from those aimed at minimizing environmental impact; (3) the choice of the final solution is influenced by the specific industrial scenario. The study specifically demonstrated that aluminium alloys can be welded with higher quality (porosity below 1% and

Equivalent Ultimate Strength up to 204 MPa) when filler wire is introduced alongside an active

wobbling scanning strategy. Conversely, filler wire can be omitted in scenarios prioritizing high-

productivity and low-carbon emissions, such as when employing a linear scanning strategy,

resulting in a reduction of equivalent carbon emissions by up to 140%.

Keywords: Laser Welding, Filler Wire, Aluminum Welding, Beam Oscillation, Carbon emission

Main Acronyms

CE_{eq}	total equivalent carbon emission
CE_e	Total carbon emissions due to electricity consumption
CE_m	Total carbon emissions due to material consumption
CE_{e-l}	Carbon emissions due to electricity consumption of laser
CE_{e-c}	Carbon emissions due to electricity consumption of chiller
CE_{e-r}	Carbon emissions due to electricity consumption of the robot
CE^s_{e-l}	Carbon emissions due to electricity consumption of laser in standby state
CE^p_{e-l}	Carbon emissions due to electricity consumption of laser during welding
CE_{eq}	total equivalent carbon emission
CE_e	Total carbon emissions due to electricity consumption
CE_m	Total carbon emissions due to material consumption
CE_{m-g}	Carbon emissions due to gas consumption
CE_{m-w}	Carbon emissions due to wire consumption
P_c^s	Chiller mean power during standby state
P_c^p	Chiller mean power during welding
$P_r^s = P_r^p = P_r$	Robot mean power
P_w^p	Power emission during wire feed motion
$t_l^s = t^s$	Standby duration of laser and chiller systems
$t_l^p = t^p$	Processing time of laser and chiller systems (equal to the welding time)
t_r^s	Standby duration of robot
t_r^p	Standby duration of laser and chiller systems
t_w^p	Wire feeder processing time (equivalent to t_l^p)
α_e	Coefficient of carbon emission for energy consumption
α_g	Coefficient of carbon emission for gas consumption
α_w	Coefficient of carbon emission for wire consumption
WL	Weld length
v_l	Laser scanning speed
Q_{gas}	Gas flow rate
v_w	wire feeding rate
r_w	Wire radius
ρ_w	Wire density

1. INTRODUCTION

Nowadays one of the main issues discussed is the environmental impact of global industrialization and the excessive use of fossil fuels, leading to increased greenhouse gas emissions and rising global temperatures. According to the International Energy Agency (IEA), global CO_2 emissions from energy combustion and industrial processes reached a record of 36.8 Gt CO_2 in 2022, a 1.5-fold increase compared to 2000 [1]. The Manufacturing sector is responsible for 5% of global CO_2 emissions, where electricity usage accounts for 35% of total energy consumption in 2021 [2]. In order to meet the net-zero emissions target by 2023, 80% of the total investment goes toward expanding the mass manufacturing capacity of renewable technologies such as wind systems and electric vehicle batteries (EV) [2]. The installed production capacity for batteries has seen a robust annual increase of 72% [2], however the energy conversion efficiency needs to be improved, as the production of a single kilowatt-hour (kWh) battery requires an energy input ranging between 40 and 60 kWh. This data highlights the need to intervene at various stages of the lithium-ion battery life cycle in order to mitigate the environmental impact, from battery manufacturing to mineral extraction and shipping. Optimizing the production process to achieve defect-free production is a feasible solution [3]. Goffin et al. [4] state that parameter selection in welding alone can produce an electrical energy saving of 60%. In this scenario paper highlights the importance of improving the energy efficiency of manufacturing processes. Specifically in large-scale automotive industries, fiber laser welding (FLW) plays a crucial role in joining thin components for battery pack parts thanks to its high precision achievable, resulting in minimal bead sizes and, notably, rapid production speeds [5]. In battery pack assembly, aluminum alloys are preferred for their cost-

effectiveness and favorable strength-to-weight ratio and advances in hybrid materials and processes, such as combining rolled aluminum with cast alloys, are explored to enhance geometric flexibility and optimize battery pack performance (i.e. optimized cooling for efficiency improving). However, welding parts that use hybrid processes such as die casting and sheet forming poses several challenges. The presence of dissolved gas in the solidified structure of die cast components facilitated pores formation, while alloys used for sheet forming commonly suffer from hot cracking [6,7]. Thus, FLW still has issues when working with aluminum alloys. Inadequate welding parameters and processes, unreliable welding monitoring, material inhomogeneities, and incorrect alignment or setup all contribute to defects in the manufacturing and assembly of battery packs. As a result, eliminating defects in battery production entirely is challenging, and although their occurrence is believed to be low, the total number of welds required for a battery pack or module multiplies this number [8]. Even though achieving defect-free production in a real-world scenario remains a significant concern, it is crucial to investigate the relationship between bead performance and energy consumption and to ensure a high-quality joint and enhanced sustainability.

2. BACKGROUND

The issue outlined and introduced in the previous section has been addressed by various authors in recent years. Several methodologies have been employed to analyze different primary goals. Life Cycle Assessment (LCA), an ISO-standardized methodology [9], is commonly used to evaluate the environmental impacts associated with manufacturing processes. This method can be classified as a problem-oriented approach and different aspects of welding have been evaluated, such as the impact of material selection [10], the choice of the welding process [11] and the end-point impact (IMPACT 2002+) [12]. Recently, Xidea et al. [13]

proposed a holistic method for comparing different welding techniques, considering three different levels of analysis: Process, Machine, and System Level. Of all the processes examined, the Machine Level, which accounts for the carbon emissions of auxiliary equipment, was found to be the most carbon-intensive. Similar conclusions are obtained from other authors. Generally, arc welding technologies that utilize a consumable electrode are more efficient and ought to be given preference. Recently, Wei et al. [14] proved that laser welding with a hot wire was more energy efficient. Feng et al [15] proposed a method to quantify energy in assembly processes by defining energy efficiency and consumption of laser arc-hybrid welding as metrics.

Other authors [16, 17] proposed an integrated decision-making model to minimize carbon emissions and processing time during cell-to-cell welding. However, since these methods do not consider the relationships that exist between product quality, feasibility and carbon emissions, they cannot be applied as decision-making techniques.

A multi-objective approach must be applied to achieve the required quality while using the least amount of energy. In literature, engineering modeling is utilized to link the quality of welds with their environmental impact [18]. This involves employing metamodeling techniques, which are also referred to as machine learning or approximation modeling [19,20]. In order to determine the relationship between energy consumption and bead geometry in fiber laser welding, Wu et al. [21] built a data-driven ensemble metamodel. Next, they used a non-dominated sorting genetic algorithm to determine the ideal process parameters, resulting in the lowest possible total energy consumption and the highest possible depth-to-width ratio of the welding bead. A fitness-sharing genetic algorithm was introduced by Yan et al. [22] to optimize processing parameters for arc welding energy conservation. However, gene

expression algorithms frequently experience early convergence, and produce unsatisfactory solutions due to their restricted local search capabilities [23,24]. To accurately depict the environment impact and evaluate process parameters, a methodical study that considers all energy sources and material usage must be built. Huang et al. [25] establish a comprehensive parameter decision model and found that the major carbon footprint is associated not with the laser source itself but with the auxiliary equipment and the cooling system. Wu et al. study [21] calculates the carbon emissions from three common welding method: laser welding, arc welding, and laser-arc hybrid welding —as well as their impact on processing performance and environmental sustainability. Tensile test results were evaluated, and factors including bead shape, microhardness, and microstructure in aluminum alloy joints were taken into account.

Additionally, an energy estimation model was developed to quantify the laser energy consumption, factoring in components such as the laser source, robot arm, cooling system, arc welding system and wire feeder system. The findings show that laser power and processing time are the dominant factors affecting energy consumption.

In this context, this research aims to overcome these challenges to elaborate the multi-characteristic of the laser welding cell and carry out the integrated decision-making of welding parameters and sequences for minimizing the carbon emission and processing time.

Following these results, this paper wants to quantify and compare the carbon emissions of different laser welding set-ups. Hence, the first part of the paper focuses on the analysis of bead quality in terms of morphology (aspect ratio), porosity and tensile-shear strength. Four laser system set-ups are analyzed combining welds with wobbling and filler wire. For each group optimal parameters were assessed. The second part of the paper wants to make a step forward, applying a parametric model that calculates for each group the environmental

impact, in terms of equivalent carbon emissions. The most influential factors on the environmental impacts, such as welding conditions, process parameters and industrial scenarios are discussed. Finally, a classification of process priority criteria is assessed throughout the quantification of quality (in terms of porosity), sustainability (in terms of CO_2, eq emissions) and industrial productivity trade-off.

Results highlight that welding with filler wire and wobbling motion is the best option for achieving the lowest porosity and maximum mechanical strength, whereas linear welding without wire is the most sustainable solution for reducing carbon footprint. Among these two scenarios, the productivity results as the trade-off criteria for defining the optimal welding setup.

3. MATERIALS AND METHODS

2.1 Laser welding

The proposed activities are carried out with the aim of comparing different laser welding methods for weld-bead optimization with different criteria priorities: i) weld bead quality, ii) process environmental impact and iii) process productivity and the overall methodology adopted is show in Figure 1. The left side of Figure 1 depicts the energy and material consumption as inputs in the system for the quantification of equivalent carbon emissions. At the top are the welding process evaluated for defining joint quality and energy utilization. The key outcomes of the trade-off analysis between quality (Section 3.1) and sustainability (Section 3.2) are presented on the right.
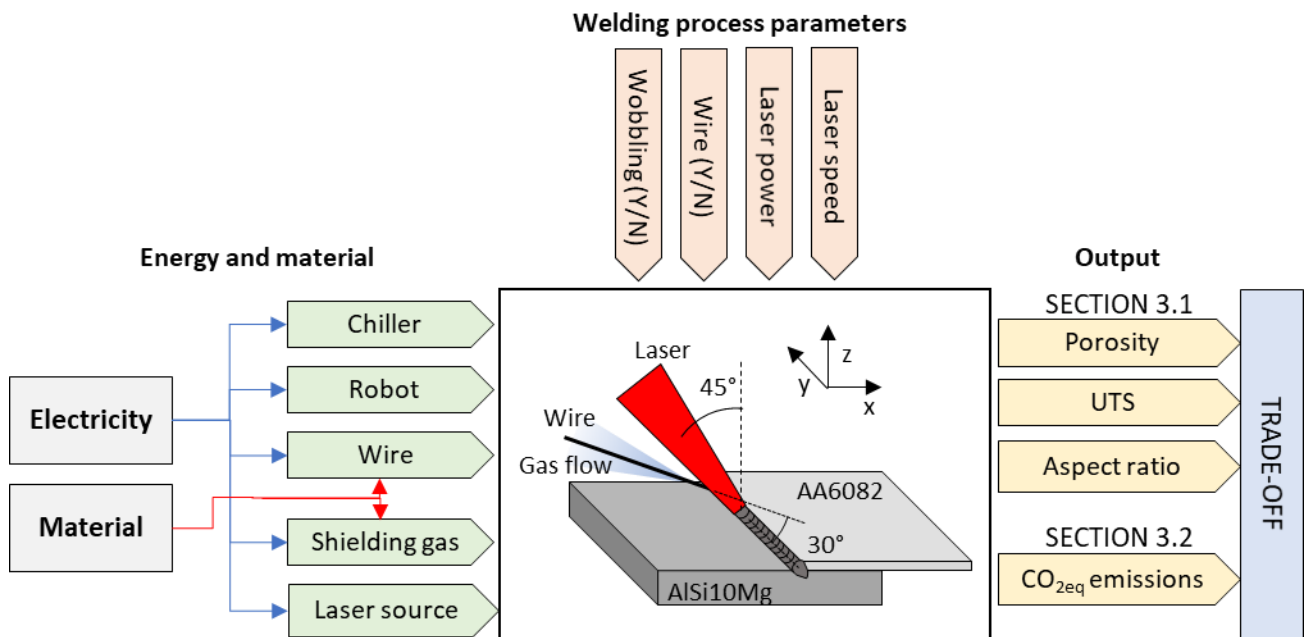
Figure 1: Methodology adopted for the laser welding process optimization following quality and sustainability criteria.

In this context four laser welding approaches are selected for comparison, including the use of filler wire and the scanning strategy (wobbling or linear). The choice of these welding conditions was based on the literature analysis [7, 26] and the available industrial laser systems [27]. For this comparison, a strategic but difficult-to-optimize weld configuration is selected. Two sheets of different aluminium alloys (AA6082 and AlSi10Mg) and produced with two different processes (hot-rolling and additive manufacturing) are welded in a lap-joint configuration. Rolled 50x50x1.5 mm AA6082 (wt.%: Cr≤0.25%, Fe≤0.5%, Mg 0.6-1.2%, Mn 0.4-1%, Si 0.7-1.3%, other elements < 0.2%, Al balance) sheet is placed on top while 50x50x4 mm AlSi10Mg (wt.%: Si 9-11%, Mg 0.25-0.55%, Fe≤0.25%, other elements < 0.2%, Al balance) sheet on bottom (Figure 1). In all configurations, laser beam moves in y direction with a 45° inclination with respect to z in x-z plane in order to achieve the welding in the corner. In the setups for which the use of filler material is planned, the wire guiding nozzle is placed ahead the laser scanner with a 30° inclination (respect

to y in y-z plane) and the filler edge directly below the beam. A Mg-rich AA5356 wire with a diameter of 1.2 mm is chosen for this experimental campaign.

The laser system employed for welding included an IPG YLS-6000 fiber source equipped with D50 two-axis scanning optics (refer to Table 1 for comprehensive specifications). The wire feed system is based on a Fronius KD7000 push-pull system, boasting a maximum feed rate of 10 m/min. The laser head is moved by a Yaskawa-Motoman HP-20 6-axis anthropomorphic robot.

Table 1: Characteristics of laser equipment.

Maximum Power	6 kW
BPP	4 mm·
Collimation focal length	200 mm
Focalization focal length	300 mm
Magnification factor	1.5
Fiber core diameter	100 μm
Spot diameter	150 μm
Maximum wobbling frequency	350 Hz

Shielding gas is a mixture of 15% He and 85% Ar with a flow rate of 30 L/min. In order to ensure that samples are in the correct position and a zero gap is obtained, a clamping device is designed and placed beneath the scanning optics.

The range of process parameters used comes from previous experimental campaign [7], considering the combination of process parameters that enable the achievement of Irradiances (ratio between Laser Power and Spot area) higher than 10 MW/cm^2 and Energy densities (product of Irradiance and Interaction time) in the order of 10^4-10^5 J/cm^2 required for welding of thick highly reflective plates. Table 2 provides a summary, with the following parameters varied for optimization: laser motion, laser power, welding speed and wire speed. A frequency of 200 Hz and an amplitude of 2 mm is employed when the wobbling approach is applied. Each test is performed with a shielding gas mixture consisting of 15% He and 85% Ar at a flow rate of 30 L/min.

Table 2: Welding process parameters divided into four categories: welding without filler wire and linear motion (Group A), welding with filler wire and linear motion (Group B), welding without filler wire and wobbling (Group C) and welding with filler wire and wobbling (Group D).

Test	Wobbling	Filler Wire	Laser power [kW]	Welding speed [mm/s]	Wire speed [m/min]
A (1-18)	N	N			/
B (1-18)	N	Y	2-3 every 0.2	25; 30; 35	1.5; 1.8; 2.1
C (1-18)	Y	N			/
D (1-18)	Y	Y			1.5; 1.8; 2.1

2.2 Power emission monitoring

Following the conclusion of the welding tests used for the geometric, microstructural, and strength characterization tests, additional tests are conducted to simulate current operating conditions. Real-time current signals from all equipment units are obtained using a current clamp, which is connected to an oscilloscope. The recorded signals in millivolts are then converted into current values by Equation 1. The current consumption of different components, such as the wire feeder, laser source, robot, laser chiller, laser head chiller, is calculated under both non-operational (standby time) and operational (processing time) conditions.

The laser and robot systems operate as balanced and unbalanced three-phase systems, respectively, while the chillers function on a single-phase system. A phyton script is used to convert the voltage data into power and then into carbon equivalent consumption, as described below. A graphical procedure scheme is shown in Figure 2.
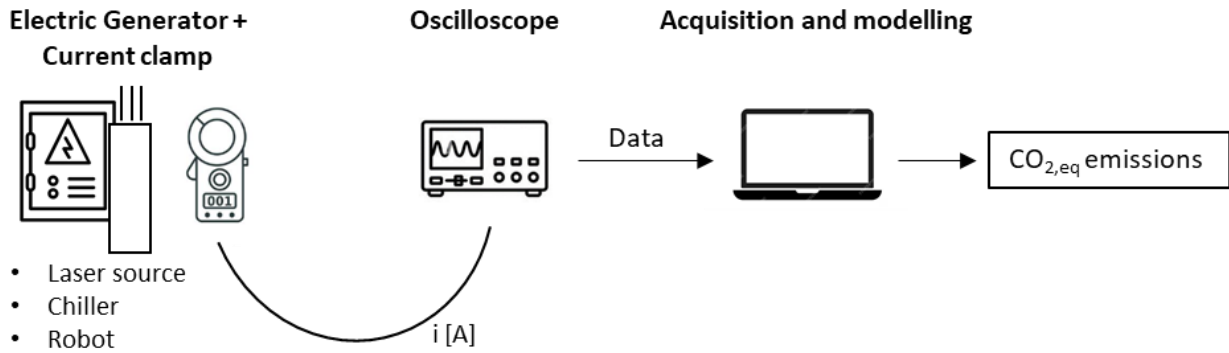
Figure 2: Signal acquisition and processing method for the evaluation of $CO_{2,eq}$ emissions

To calculate the effective current value, the voltage signal is converted using the formula:

(1) $I = \frac{voltage\ signal\ [mV]}{S}$ [A]

where S represents the sensitivity of the amperometry clamp, set as 10 mV/A. The root mean square (RMS) method is employed to compute the effective current signal in the system [28]:

(2) $I_{RMS} = \sqrt{\frac{1}{N} * \sum_{i=1}^{N} I_i^2} = I_\phi$ [A]

Here, I_i is the current value at each point of the signal, and N is the total number of points in the signal. The total active (real) power in the chiller's *single-phase system* $P_{s,tot}$ is calculated as follows [27]:

(3) $P_{s,tot} = P_\phi = V_\phi * I_\phi * cos\theta$

Where V_ϕ represents the phase voltage (230V), I_ϕ is the current of the phase and θ denotes the phase difference between voltage and current.

In the case of the *three-phase symmetric and balanced* system, characterized by equal line currents ($I_{\phi 1} = I_{\phi 2} = I_{\phi 3} = I_L$), the total active power $P_{t,tot}$ is the sum of each phase's active power:

(4) $P_{t,tot} = 3\,P_\phi = 3\,V_\phi * I_L * cos\theta$

To express $P_{t,tot}$ in terms of line voltage ($V_L = 400V$) and line current, the equation is:

(5) $P_{t,tot} = \sqrt{3} * V_L * I_L * cos\theta$

A power factor cosθ is close to 1 indicates good energy efficiency in the system. The power factor cos(ϑ) can be calculated using real power RP (40 kW) and imaginary power IP (6 kVAr):

(6) $cos(\vartheta) = \frac{RP}{\sqrt{RP^2+IP^2}} = 0.98$

The values of RP and IP were taken from the electric panel while the laser system was working. In the case of a *three-phase unbalanced system*, where the current values in the three conductors of robot system differed, the following consideration is made:

(7) $P_{t,tot} = P_{\phi1} + P_{\phi2} + P_{\phi3} = \sum_{i=1}^{3} V_\phi * I_{\phi i} * cos\theta$

Where V_ϕ is 230V (legal standard CEI 8-9) and $I_{\phi i}$ is the current for each phase.

Using Equations 3,5 and 7, the power absorbed by each component are assessed with varying power and speed, as detailed in Table 2.

2.3 Weld bead characterization

Following the experimental tests, middle cross-sections of the welded samples are prepared by hot mounting samples in resin and polishing the final surface with 800-2500 grit SiC followed by 1-0.05 µm alumina in suspension. Samples for microstructural analysis are then etched with Keller's reagent (1 ml HF, 1.5 ml HCL, 2.5 ml HNO3 and 95 ml H2O) for 20 s to prepare them for initial examination. The primary geometric characteristics of the weld bead are assessed using optical microscopy (OM, Nikon Optiphot-100), with the average porosity determined via image processing using ImageJ open-access software. Mechanical characterization is performed after contouring the

welded samples to achieve a total length of 80 mm, overlap of 10 mm and width of 25 mm. Room

temperature tensile-shear tests are carried out using a hydraulic testing machine (Italsigma S.r.l,

Forlì, Italy) with a 20 kN load cell. The strain rate is set to 2.8·10-4 s-1 and fixed using a constant

cross-head separation rate of 1 mm/min.

2.4 Carbon emission model

The equivalent carbon emission of laser welding is calculated with the main scope of highlighting

the difference due to the adopted welding strategy. Other papers describe the method for carbon

emission calculation [21,30] in laser welding, so a summary of this model is here described with

the appropriate specifications relating to the welding strategy. The proposed model follows a

hierarchical scheme, and at the top position, there is the total equivalent carbon emission (CE_{eq})

calculated by summing the contribution of carbon emission due to direct energy consumption

(CEe) and the material consumption (CEm) (Equation 8).

(8) $CE_{eq} = CE_e + CE_m$

2.4.1 Energy consumption contribution

Starting from the analysis of CE_e, contributions are considered from all the involved items. In all

the laser welding setups mentioned, including the laser source (l), chillers (c), and robot (r), their

respective contributions were assessed, along with the energy consumption of the wire feeder

when the filler wire is active. Therefore, for tests belonging to Groups A and C, CE_e is calculated

with Equation 9, while Groups B and D require Equation 10.

(9) $CE_{e(A,C)} = CE_{e-l} + CE_{e-c} + CE_{e-r}$

(10) $CE_{e(B.D)} = CE_{e-l} + CE_{e-c} + CE_{e-r} + CE_{e-w}$

The energy contribution of each system is then detailed. Starting from laser beam generation, the required energy differs between the standby state (CE_{e-l}^{s}), when the pumping system is active and the laser is ready, but it is not emitting and the welding phase CE_{e-l}^{p}. Equation 11 described as the authors evaluate those two energy states.

$$(11)\ CE_{e-l} = CE_{e-l}^{s} + CE_{e-l}^{p} = \alpha_e \left(P_l^{s} \cdot t_l^{s} + P_l^{p} \cdot t_l^{p} \right)$$

P_l^{s} and P_l^{p} are the laser mean active powers calculated, respectively, during the standby and welding state. The power of standby status P_l^{s} is constant, while the power of processing status P_l^{p} depends on welding laser power. t_l^{s} and t_l^{p} denote the standby duration and processing time, respectively. Consistently with the respective powers, the value of t_l^{s} was kept constant across all processes (set to 1 min). In contrast, t_l^{p} is contingent on process parameters, particularly the welding speed, as illustrated in Equation 12.

$$(12)\ t_l^{p} = \frac{WL}{v_l}$$

Where w_L is the weld length and v_l is the laser scanning speed.

Finally, α_e is the coefficient of carbon emission for electricity consumption and it is reported in Table 3. The analysis of both the laser-head chiller and laser-source chiller employed identical methodology.

Table 3. Relevant coefficients of carbon emission

α_e	0.267 kgCO$_{2eq}$/kWh	[31]
α_{gas}	0.611 kgCO$_{2eq}$/m^3	[32]
α_w	15.1 kgCO$_{2eq}$/kg	[33]

The chiller serves the crucial function of maintaining the designated components at a prescribed temperature range. During welding, the pump periodically activates, and the chiller remains on

standby during non-operational intervals. The duration and the frequency pump activation of the cooling system are dictated by the process chain. By aligning the operational periods of the laser with those of the chillers, a simplified condition is considered. Based on this consideration, the energy consumption of each chiller can be calculated using Equation 13.

$$(13)\ CE_{e-c} = \alpha_e \big(P_c^s \cdot t_l^s + P_c^p \cdot t_l^p\big)$$

Where P_c^s and P_c^p are the chiller mean powers calculated, respectively, during the standby state and welding.

The robot's energy consumption is the final contribution that is present in all laser welding scenarios. According to earlier considerations, the power for this motion system must be measured when it is in the running (P_r^p) and standby states (P_r^s), with the resulting carbon emission calculated using Equation 14.

$$(14)\ CE_{e-r} = \alpha_e \big(P_r^s \cdot t_r^s + P_r^p \cdot t_r^p\big)$$

The duration of the robot's standby and moving states is denoted as t_r^s and t_r^p. These durations differ from the laser and chiller ones because, before laser emission, the robot reaches the initial welding position from a safety position, which is different from the previous one. Due to the negligible difference in consumption of the robot between the operating phase and the standby phase, this variance was neglected and Equation 14 was simplified as follows:

$$(14b)\ CE_{e-r} = \alpha_e \cdot P_r \cdot (t_r^p + t_r^s)$$

Moreover, for Groups B and D the contribute of wire feeder (CE$_{e-wire}$) is considered. Due to the low current value request from this equipment, no specific measures are carried out and a maximum value of 6 A is included in the calculations, resulting in a constant power emission (P_w^p in Table 5). The final contribution is formulated as follows:

(15) $CE_{e-w} = \alpha_e\left(P_w^p \cdot t_w^p\right)$

Where t_w^p is equal to t_l^p.

2.4.2 Material consumption contribution

The calculation of emissions resulting from material usage (CE$_m$) takes into account the *wire* for

Groups B and D as well as shielding gas for all set-ups.

The application of shielding gas during welding is needed to wipe away the generated plasma,

mitigating the oxidation of the weld seam. As a result, this procedure guarantees the achievement

of a high-quality weld bead. The gas usage is found to have a minimal contribution on the overall

quantity of carbon emissions in accordance with Equation 16:

(16) $CE_{m-g} = \alpha_{gas}(Q_{gas} \cdot t_l)$

Where α_{gas} and Q_{gas} are, respectively, the coefficient of carbon emission for shielding gas

consumption (see Table 3) and the flow rate. The welding and gas supply times coincide.

Regarding the influence of wire consumption on carbon emission outcomes, the impact can be

quantified through Equation 17:

(17) $CE_{m-w} = \alpha_w(v_w \cdot t_l^p \cdot \pi \cdot r_w^2 \cdot \rho_w)$

where α_w is the coefficient of carbon emission associated with wire consumption (refer to Table

3), v_w is the wire feeding rate, t_l^p is the welding time (the feeding wire time is approximately

equivalent to the duration of processing status), r_w is the radius of the wire, and ρ_w represents the

metal density of the wire. The values of the wire's radius and density are constant and equal to 0.6

mm and 2.64 g/cm³, respectively.

2.5 Evaluation criteria and trade-off

The trade-off between welding strength and process carbon emissions during laser welding is assessed using the straightforward graph in Figure 3. To begin the analysis, it's crucial to grasp the prerequisites that need to be met. If ensuring mechanical resistance (minimizing defects) is paramount, porosity becomes the primary selection criterion. Consequently, two distinct and opposing scenarios emerge:

i)   Strict prerequisites: This implies high-quality weld beads with porosities less than 1%.

ii)   No prerequisites: Porosity levels higher than 4% are acceptable because there are no strength requirements.

While the first scenario prioritizes welding quality, the second scenario focuses more emphasis on process sustainability.
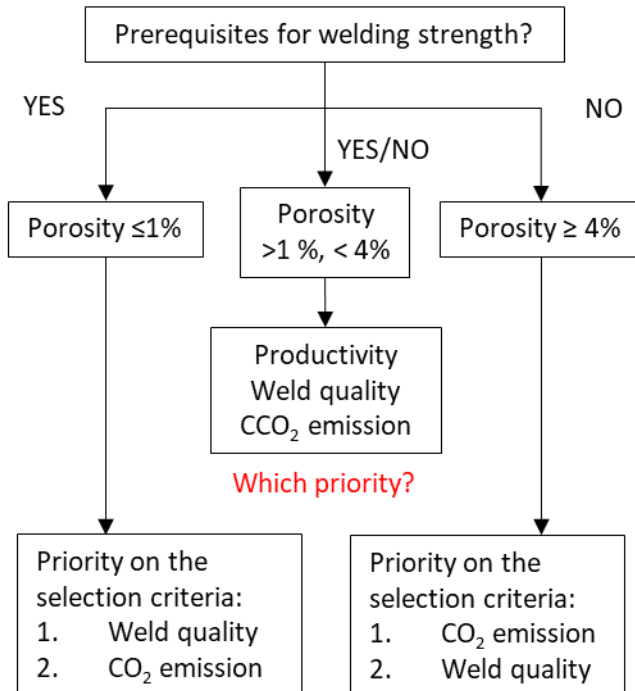

Figure 3: Priority of the selection criteria as the requirements and industrial scenario change

The specific industrial scenario defines which of these approaches should be prioritized if there are not prerequisites, making the tradeoff between these criteria even more relevant. In this scenario, industrial productivity plays the main role. It is measured as the ratio between the standy time ($t^s_l = t^s$) to the production time ($t^p_l = t^p$)

This ratio helps classify industrial scenarios as either highly productive ($t^p \gg t^s$) or low productive ($t^s \geq t^p$). In light of the resulting values, a definitive priority selection criterion is established.

3. RESULTS

3.1 Welding process optimization

The welding quality is assessed in the four conditions (A, B, C, D) by a first evaluation of the weld bead porosity. A preliminary screening process is conducted by analyzing the graph in Figure 4. The porosity percentage was categorized into four classes, aligning with the ISO 13919-1 standard: 1) 0-2%, 2) 2.1-4%, 3) 4.1-6% and 4) >6 %. The number of joints belonging to each class (in percentage terms) is used to define the bar's height. For example, Group A has 5.6% of specimens tested with less than 2% porosity. It is clear that all samples welded without filler wire and with wobbling motion (Group C) show medium or high levels of porosities, with nearly 80% of the samples falling into class 4.
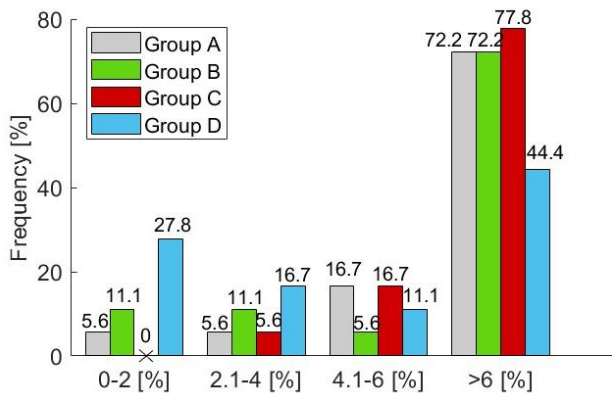
Figure 4: Frequency of sample identification based on porosity class in the four analyzed process conditions (Groups A, B, C, D).

Conversely, joints carried out with filler wire and wobbling motion (Group D) demonstrate that 45% of process conditions result in very low porosity (porosity <4%). Finally, Groups A and B exhibit a narrow operating window yielding excellent qualities.
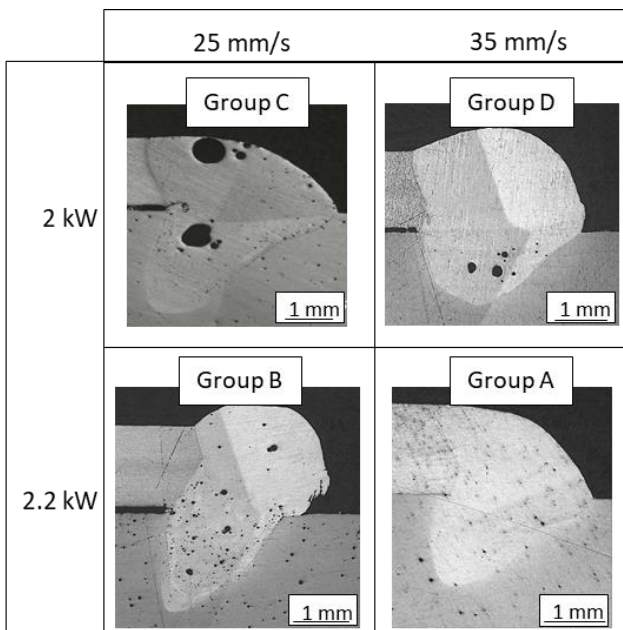

Figure 5: Lower-class porosity weald beads for each condition: group A) 2 kW, 35 mm/s; B) 2.2 kW, 35 mm/s; C) 2 kW, 25 mm/s; D) 2.2 kW, 25 mm/s.

However, despite the relevance of these results, other aspects should be contemplated, such as the bead's quality and process speed. Figure 5 illustrates micrographs of the optimal weld beads

obtained for each condition. To attain the best possible weld quality with the least amount of pore formation, low energy input, or lower power, must be set.

The application of linear motion, applied in Groups A and B, speeds up the welding process and minimize porosity in the weld. Even more pronounced is the influence of laser motion on weld-bead geometry, as wobbling results in a reduced aspect ratio (weld depth/weld width = D/W). Comparing the samples of Groups B and D (with wire), the mean aspect ratio is 0.83 (max=1.09, min=0.67) with linear motion and 0.45 (max=0.55, min=0.34) with wobbling. Direct interaction between the laser beam and sheets (Groups A and C) also allows a wider melt pool to be achieved with linear motion. With beam wobbling, the resulting mean weld aspect ratio is 0.57 (max=0.64, min=0.48), while linear motion leads to mean value of 0.42.

These findings confirm that wobbling has a great impact on the weld bead's morphology, with this effect being more significant in welding with filler wire. Moreover, the employment of wobbling without filler wire increases turbulence in the melt pool, which raises porosity without providing any advantages that would justify its use. Regarding the relationship between weld bead morphology and process variables, lower welding speeds and higher powers lead to larger widths in all tested conditions. Following the investigation of the weld bead micrographs, tensile-shear tests were performed on samples, one for each group, that had been welded using the most effective process parameters (summarized in Table 4). The aim was to measure the maximum failure load and equivalent ultimate strength allowing these values to be correlated with the process parameters and the process emissions.

Table 4: Welding process parameters selected for tensile-shear tests.

Group	Wobbling	Filler Wire	Laser power [kW]	Welding speed [mm/s]	Wire speed [m/min]
A	N	N	2	35	/
B	N	Y	2.2	35	2.1
C	Y	N	2	25	/
D	Y	Y	2.2	25	1.5

Preliminary tests manifest the lowest values of strength for Group C, hence those samples were not included in the mechanical characterization process. Tensile shear test findings agreed well with the weald bead characterization data. With a mean failure load of 5.9 kN and a standard deviation of 0.37, the samples from Group D demonstrated the maximum strength. Following in descending order of strength values, Group A samples could withstand loads of up to 5.3 kN with a standard deviation of 0.18. Follow the samples of Group B, which exhibited a mean failure load of 4.8 kN (standard deviation of 0.14). Similar considerations can be made in relation to the equivalent ultimate strength. Figure 6 presents the Equivalent Ultimate Strength (US) of the same four samples, where it can be seen that similar values are achieved in each case. Group D samples exhibit a higher mean value of US by a factor of 1.07 compared to Group B samples, which achieve the lowest mean value.
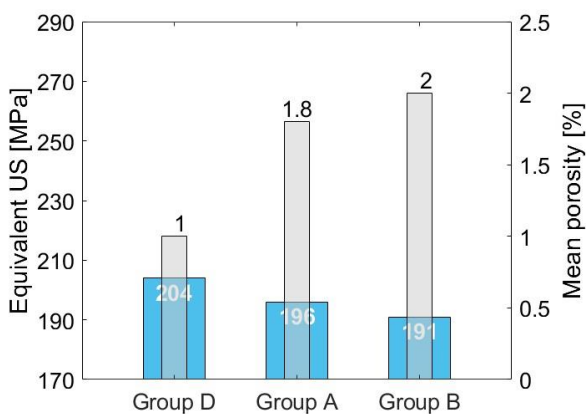

Figure 6: Results of tensile-shear tests in terms of Equivalent Ultimate Strength.

3.2 Carbon emission analysis

The active powers calculated with the method described in Section 2.2 are reported in Table 5. Laser active power, in operative condition, depends on the selected welding laser power, while the other assessed active powers remain constant. It's also important to highlight that the robot's active power always assumes similar fixed value, whether it's in standby or operational mode.

Table 5. Active powers measured during welding process.

Welding Power [kW] Active power	2	2.2	2.4	2.6	2.8	3
P_l^p	7.82	9.06	9.89	10.41	11.30	12.56
P_c^p	2.76					
P_r^p	0.48					
P_w^p	0.28					
P_l^s	1.30					
P_c^s	0.72					
P_r^s	0.48					

The power consumption of the chiller unit encompasses both the refrigeration of the laser source and the chiller for the laser head. Utilizing active power values, the equivalent carbon emissions were calculated for each equipment across process conditions. These values are influenced by the welding length and laser scanning speed during operational phases and the standby time during equipment idle periods. CO_2 emissions from gas assistance make an exception: they are associated with process duration, laser speed, and weld length (WL) even if they are classified as non-operational. While standby time and WL are dependent on the specific industrial scenario, the laser speed value comes from the optimization process previously stated. In summary, three main factors are considered: i) welding condition, ii) process parameters, and iii) industrial scenario.

3.2.1 Influence of process parameters on CEeq

In this sub-section the effect of power and speed was mainly considered, without taking into account the actual optimized parameters which will be the subject of analysis and comparison in paragraph 3.3.2. Table 6 summarized the calculated values for welding without filler wire for the overall range of power and speed, considering a unit welding length (1 m) and a unit standby time (1 min). The impact of process parameters on total carbon emissions (CEeq) can be elucidated by referencing the data in Table 6 and examining the corresponding graph in Figure 7. The effect of power is represented by the comparison of bars 1 and 3 (or 2 and 4), obtained, respectively, using the minimum (2 kW) and the maximum (3 kW) power. Welding power has a direct influence only on the emissions resulting from the use of the laser, both in operational and non-operational conditions. The absolute values of equivalent carbon emissions CEeq remain constant for all other components within the system. However, this leads to a reconfiguration in the relative percentage contributions to the total value. Specifically, as laser power increases, laser consumption becomes predominant, constituting over 50% of the total emissions. Analyzing the impact of laser speed (bars 1 and 2 or 3 and 4), each component displays variability in emission contribution during the welding phase while maintaining a similar weight of each equipment.

Table 6. Carbon emissions calculations for various parameters in welding without filler wire.

P_l [kW]	v_l [mm/s]	CE^p_{e-l} [g]	CE^p_{e-r} [g]	CE^p_{e-c} [g]	CE^p_e [g]	CE^s_{e-l} [g]	CE^s_{e-r} [g]	CE^s_{e-c} [g]	CE_{m-g} [g]	CEeq [g]
2	25	23.20	1.42	8.19	32.81				12.22	57.29
	30	19.33	1.18	6.82	27.34				10.18	50.79
	35	16.57	1.02	5.85	23.44				8.73	45.43
2.2	25	26.88	1.42	8.19	36.49				12.22	61.97
	30	22.40	1.18	6.82	30.41				10.18	53.85
	35	19.20	1.02	5.85	26.06				8.73	48.05
2.4	25	29.34	1.42	8.19	38.95				12.22	64.43
	30	24.45	1.18	6.82	32.46				10.18	55.91
	35	20.96	1.02	5.85	27.82	5.79	4.27	3.20	8.73	49.81
2.6	25	30.88	1.42	8.19	40.50				12.22	65.98
	30	25.74	1.18	6.82	33.75				10.18	57.19
	35	22.06	1.02	5.85	28.93				8.73	50.92
2.8	25	33.52	1.42	8.19	43.14				12.22	68.62
	30	27.94	1.18	6.82	35.95				10.18	59.39
	35	23.95	1.02	5.85	30.81				8.73	52.80
3	25	37.26	1.42	8.19	46.87				12.22	72.35
	30	31.05	1.18	6.82	39.06				10.18	62.51
	35	26.62	1.02	5.85	33.48				8.73	55.47

From a comprehensive perspective on CEeq, the maximum expected difference between the selected processes parameters— thus from delivering the minimum energy (2 kW, 35 mm/s) and the maximum energy (3 kW, 25 mm/s) —amounts to 26.9 g. This signifies a 59.4 % increase from the first set of parameters to the second. The proportions of carbon emissions depicted in Figure 7 facilitate the identification of the extent of influence of power and speed on the laser generation system (laser source), chillers, robot, and shielding gas. The motion system and chillers in standby status are solely influenced by laser speed (i.e., the welding time), and the associated range of variation is negligible, as mentioned earlier. The robot maintains low emissions even during welding, contributing less than 10%, whereas chiller consumptions become more significant when the pump and compressor are active (operative state).
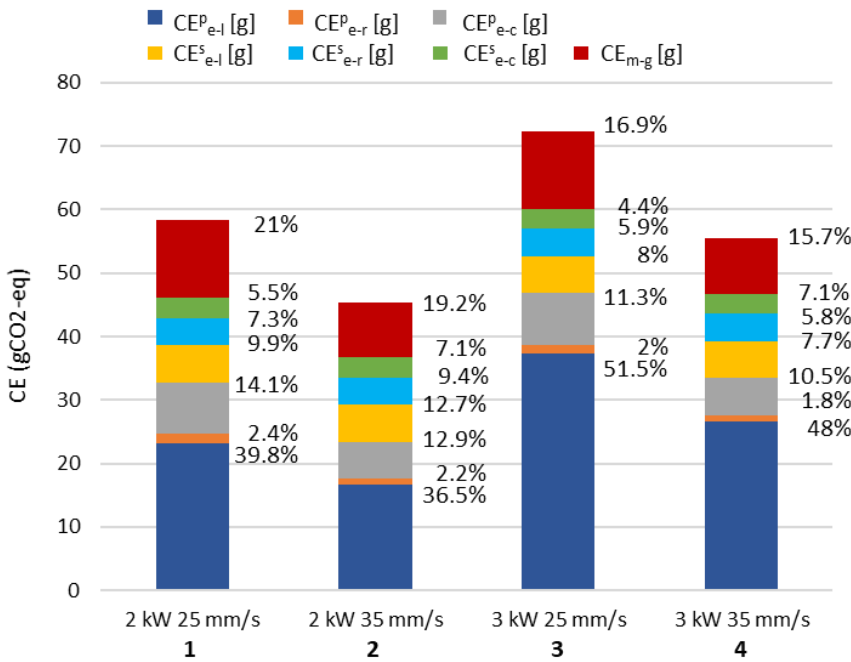
Figure 7. Equivalent carbon emissions for different process parameters in welding without filler wire.

Notably, the combined carbon emissions from the laser and shielding gas constitute up to 68%.

Analyzing the variation in the average CEeq response for input variables at different levels, it can be asserted that welding speed exerts the most substantial impact (refer also to Figure 8).
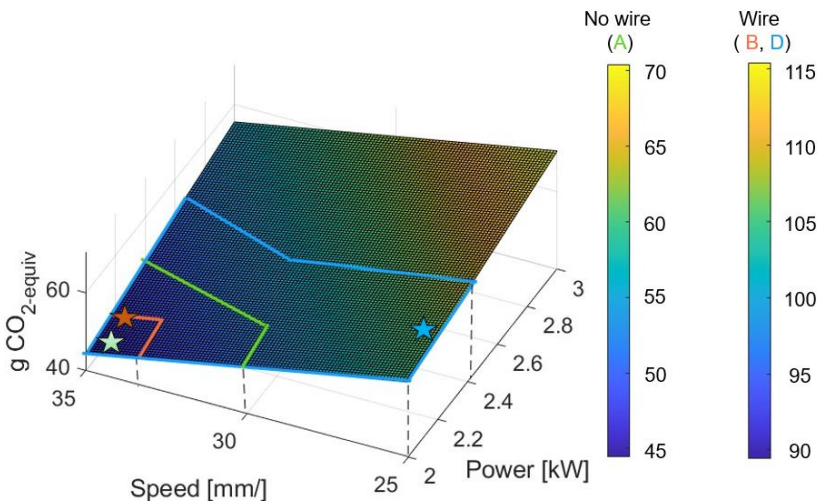

Figure 8. Influence of laser speed and power when welding without filler wire. Welding speed exerts the most significant influence.

Specifically, the difference between the average CE values obtained at 2 kW and 3 kW is 11.9 gCO2eq, while the disparity between the mean CE values calculated at 25 mm/s and 35 mm/s is 14.9 gCO2eq. Figure 8 show also the process parameters effect on the specific welding condition. Identifying a working area in which resulting welds are characterized by porosity less than 4% (green area for A welds, orange for B and light blue for D), the graph highlights as this area increase from B set to D set. However, considering the higher quality level of each condition (colored star) the carbon emission increases in the same direction (maximum value for D setup and minimum for A setup). Everything stated so far can also be extended to the case of welding with filler material. Table 7 and Figure 9 show the calculation performed for these welding conditions.

Table 7. Carbon emissions calculations for various parameters in welding with filler wire.

P_l [kW]	$v_l - v_f$ [mm/s - m/min]	CE^p_{e-l} [g]	CE^p_{e-r} [g]	CE^p_{e-w} [g]	CE^p_{e-c} [g]	CE^s_{e-l} [g]	CE^s_{e-r} [g]	$CE_{m.w}$ [g]	CE^s_{e-c} [g]	$CE_{m.g}$ [g]	$CEeq$ [g]
2.0	25-1.5	23.20	1.42	0.82	8.19					12.22	105.22
	30-1.8	19.33	1.19	0.68	6.82					10.18	97.58
	35-2.1	16.57	1.02	0.58	5.85					8.73	92.12
2.2	25-1.5	26.88	1.42	0.82	8.19					12.22	108.90
	30-1.8	22.40	1.19	0.68	6.82					10.18	100.65
	35-2.1	19.20	1.02	0.58	5.85					8.73	94.75
2.4	25-1.5	29.34	1.42	0.82	8.19					12.22	111.36
	30-1.8	24.45	1.19	0.68	6.82					10.18	102.70
	35-2.1	20.96	1.02	0.58	5.85	5.79	4.27	46.11	3.20	8.73	96.51
2.6	25-1.5	30.88	1.42	0.82	8.19					12.22	112.91
	30-1.8	25.74	1.19	0.68	6.82					10.18	103.98
	35-2.1	22.06	1.02	0.58	5.85					8.73	97.61
2.8	25-1.5	33.52	1.42	0.82	8.19					12.22	115.55
	30-1.8	27.94	1.19	0.68	6.82					10.18	106.18
	35-2.1	23.95	1.02	0.58	5.85					8.73	99.50
3.0	25-1.5	37.26	1.42	0.82	8.19					12.22	119.28
	30-1.8	31.05	1.19	0.68	6.82					10.18	109.30
	35-2.1	26.62	1.02	0.58	5.85					8.73	102.17

The considerations previously discussed regarding process parameters remain applicable even in welding with filler material. However, the introduction of wire, which involves significant material consumption, alters the order of importance for energy consumption. In this welding condition, the CEeq are predominantly influenced by the wire, accounting for up to 50 %, whereas the energy consumption of beam generation becomes less significant. The value CE_{m-wire} in gCO_{2eq} is correlated with the welding length, and as a result, it remains constant for all the process conditions in this scenario. Further discussions on this matter will be provided in Section 3.2.3.
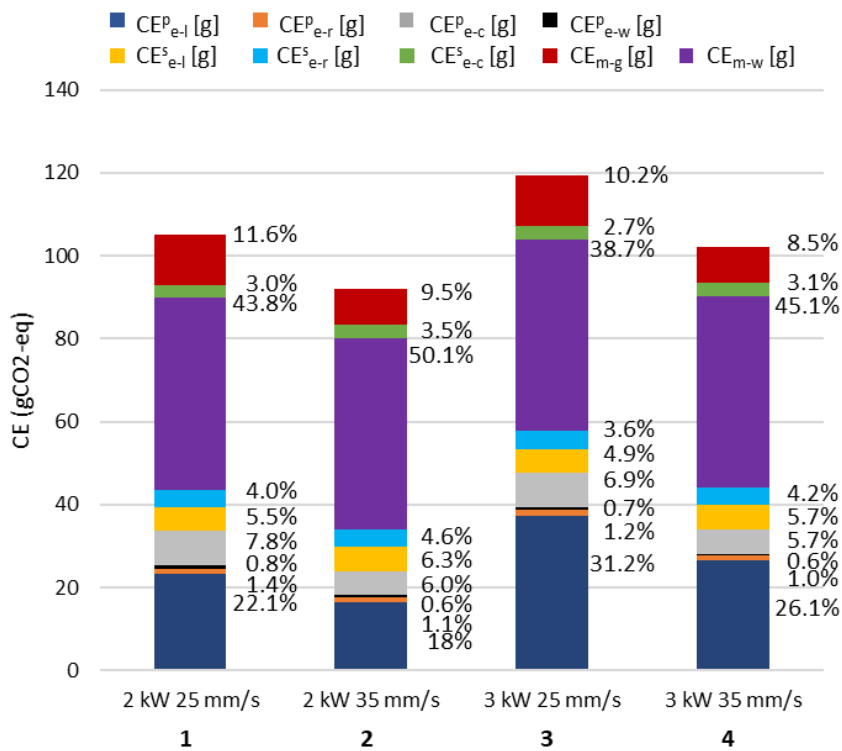

Figure 9. Equivalent carbon emissions for various process parameters in welding with filler wire.

3.2.2 Influence of welding condition on CEeq

This section shows and compares the CEeq values calculated using the optimized process parameters listed in Table 4. Figure 10a shows the carbon emissions for each Group's optimum

weld. The comparison of bar heights shows how employing filler wire has a negative effect on the process' sustainability, with total CEs rising by as much as 140%.

Specifically, as detailed in Section 3.1, if filler wire is used, the wobbling motion emerges as the most effective technological choice, exhibiting very low porosity and a smaller aspect ratio. These conditions in Group D, however, have the most significant environmental impact. Groups A and Group C are almost equivalent in terms of carbon emission. Despite the comparable emissions, the low-quality weald beads obtained for Group C do not make it a viable alternative.
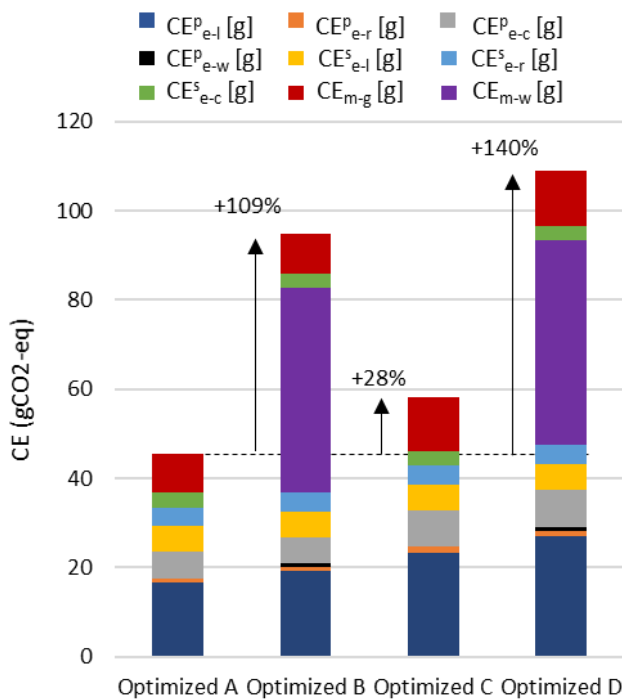

Figure 10. Influence of factors involved in calculating equivalent carbon emission of the optimized welding conditions. The use of filler wire is ranked first, with an increase of 109% for Group B and of 140% for Group D, followed by laser speed, which shows a +28% increase in Group C.

From Figure 10, it is also possible to establish an order of influence among the factors involved: filler wire emerges as the most influential variable, followed by laser speed. Laser speed is related to scanning strategy because optimized welding with wobbling requires lower laser speed and,

consequently, longer welding time. Due to the minimal impact of power on equipment other than the laser source and the extremely low variability of these parameters between optimal conditions, laser power is consequently ranked third in terms of influence.

3.2.3 Influence of the industrial scenario on CEeq

To further examine the calculated data of CE, some consideration about the effect of specific products and industrial scenarios can be made, without claiming to analyze in detail a specific case study but drawing general considerations. As mentioned before the laser-material interaction phase (or operational phase) is defined as the duration of laser beam emission for allow sheets welding (t_l^p). However, the duration of the whole process consists of two parts: the interaction phase and the standby phase, during which some complementary operations can be performed. For example, this stage encompasses the movement of the components out of the assembly line and the arrival of the new parts to be welded.
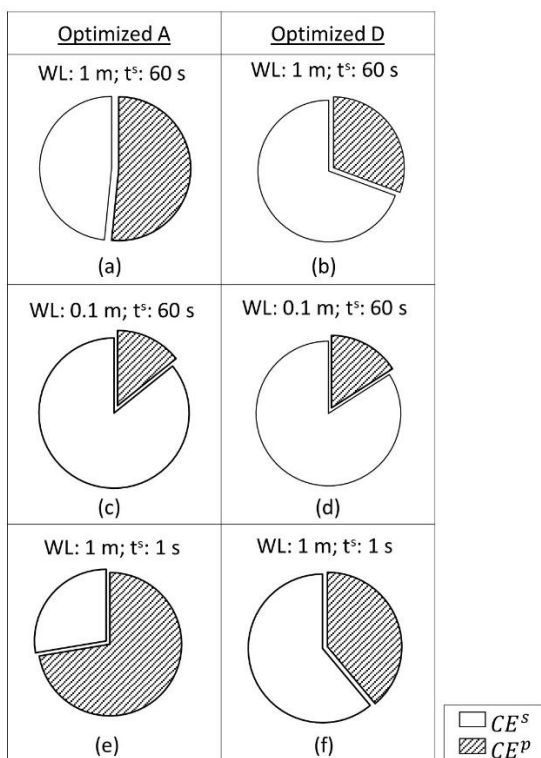

Figure 11. Contribution of CE in operational and standby phases

The relevance of equipment consumption in these two phases is strictly correlated to the welding length and the standby time and the correlation is highlighted in Figure 11. Two welding conditions were selected for this comparison: welding performed with the optimized parameters defined for Group A (No wobbling, no wire) and Group D (wobbling and wire), respectively shown on the left and right side of Figure 11. Then the equivalent CE proportion between non-operational and operational phases was respectively salmon pink and light green colored for three combinations of welding length WL and standby time: i) WL: 1 m, t^s: 1 min (Figure 11a,b), ii) WL: 0.1 m, t^s: 1 min (Figure 11c,d) and iii) WL: 1 m, t^s: 1 s (Figure 11e,f).

By reducing the stand-by time and extending the welding length WL (Figures 11c and 11e), resulting in a longer processing time, the percentage of energy consumption and CE attributable to welding increases, thus contributing more significantly to the overall carbon emissions.

In absence of filler wire the standby time is less relevant on the consumption balance between operational and non-operational phases (comparison between Figures 11 b,d,f). This result explains also the more pronounced effect of non-operation phase of Group D respect to Group A, that is due to the wire. Figure 12 shows the gCO2eq for welding processes without filler wire at different power, speed, and weld lengths. When examining the final values of CEeq, WL on the x-axis exhibits the most pronounced influence.
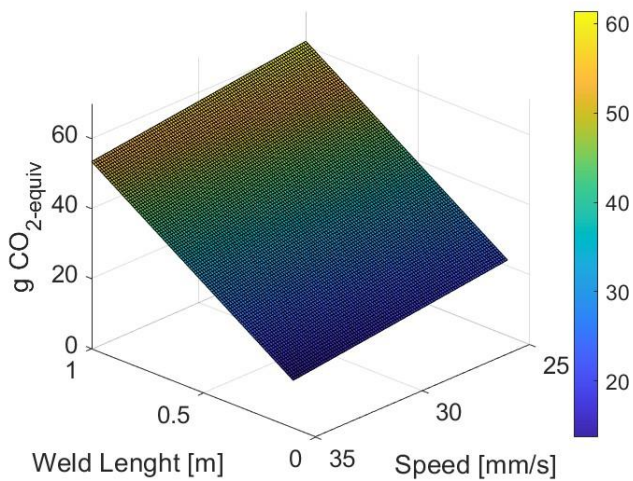
Figure 12. Influence of laser speed and weld length when welding with filler wire. The weld length is the variable that exerts the most significant influence.

Nevertheless, with an increase in WL, the impacts of power and laser speed also intensify. Indeed, as WL rises, the slopes of the lines defining the CEeq ranges decrease, indicating a more effective control of speed on process consumption.

3.3 Selection criteria for welding setup definition

Referring to the results presented in the previous paragraphs, it is now possible to define more easily which welding conditions to consider optimal in the various scenarios outlined in Figure 3. If the prerequisites to the process are stringent, the primary selection criterion is joint quality. In this situation, as highlighted in paragraph 3.1 (particularly through Figure 4), the optimal welding condition will involve the use of filler material and the wobbling motion strategy (Group D). Conversely, if there are no requirements regarding the mechanical strength of the joint, the primary selection criterion, as mentioned earlier, can be related to minimizing CO_2 emissions. Following the results of paragraph 3.2.2, the choice will then fall on welding without filler material and linear motion (Group A).

These two opposing options encompass a wide range of "intermediate" cases, where no clear initial constraint is declared. In this scenario, the industrial context serves as the guiding principle for action. Plant productivity can thus be incorporated among the selection criteria for the welding process. Following the results of paragraph 3.2.3, the industrial scenario can be characterized by either a low or high-productivity plant, depending on the ratio value between the processing time t^p and standby time t^s.

By analyzing the results obtained when all the three criteria are included (Figure 13), namely i) productivity, ii) weld quality, and iii) CO2 emissions, it becomes evident how productivity can serve as an excellent trade-off criterion.
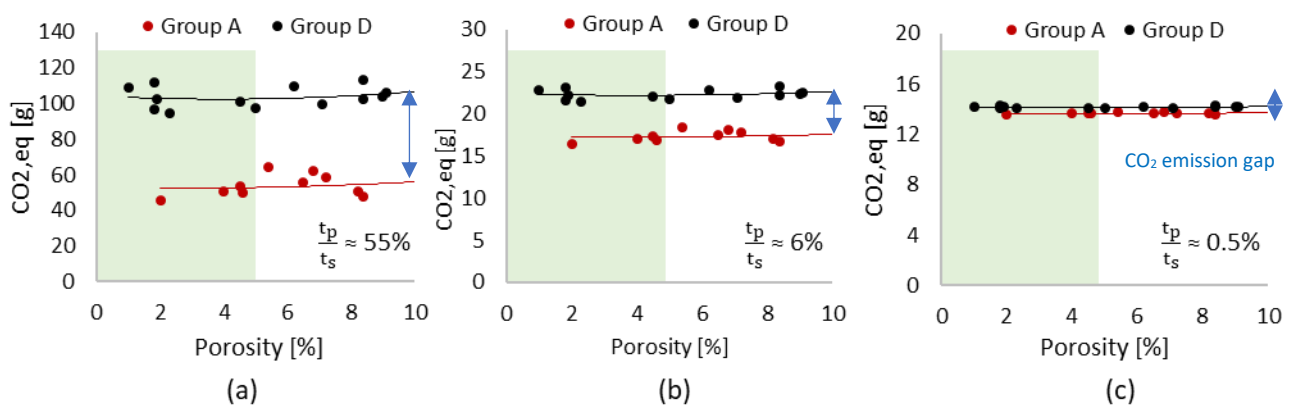

Figure 13. Analysis of the trade-off in the choice of welding condition.

Figure 13a) displays a CO_2 emissions/porosity graph obtained by calculating the emissions produced by welds from groups A and D in a plant with a process-to-standby time ratio of 55% (WL=1m, t^s=60s). Figures 13b) and 13c) present the same data calculated for t^p/t^s ratios of 6% (WL=0.1 m, t^s=60s) and 0.5% (WL=0.01 m, t^s=60s), respectively. By looking at data, it is evident that a decrease in productivity (lower t^p/t^s ratios) leads to the convergence of the two $CO_{2,eq}$ curves for A and D weld groups. The emission gap (ratio between $CO_{2,eq}$ of group A and group D) between these two welding modes decreases from higher t^p/t^s ratios (Figure 13a) to lower t^p/t^s

ratios (Figure 13c). Assuming that $CO_{2,eq}$ gap emission variation is set below 10%, the two curves,

hence the two processes, can be considered comparable due to the simplifications of the model

applied. Hence, a t^p/t^s ratio of 2% can be identified as a fair trade-off value. The framework

presented in Figure 3 can thus be completed and redefined based on the results obtained, as
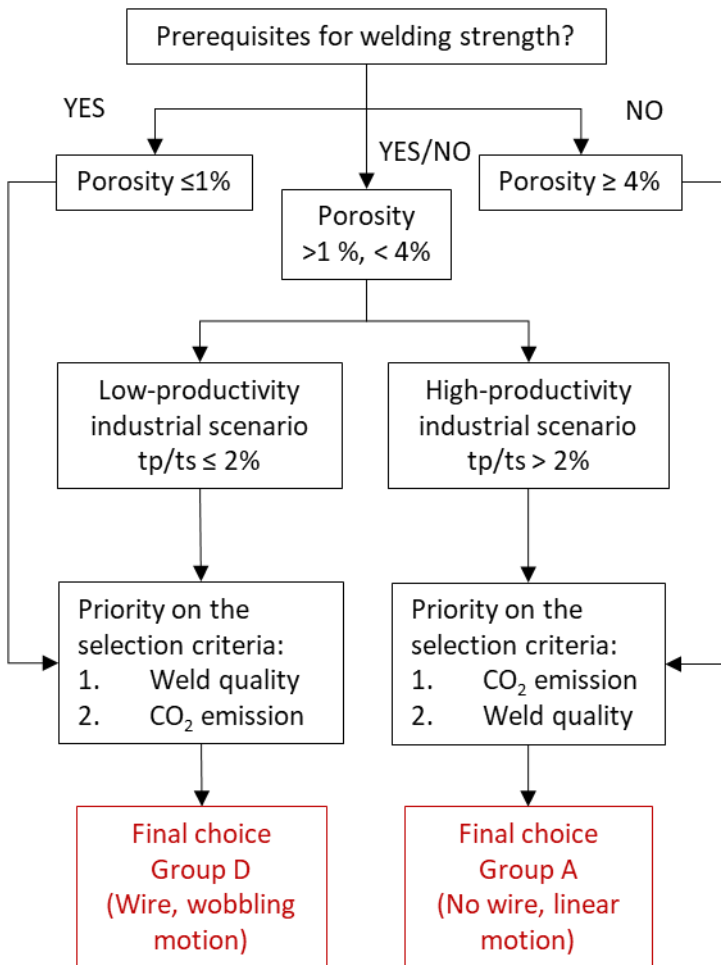
illustrated in Figure 14.

Figure 14. Final definition of priority in the selection criteria

4. DISCUSSION

One of the main issues currently facing laser welding of dissimilar aluminum alloys is the definition

of a sustainable industry-ready process capable of assuring high quality joints with good

productivity. In the light of this challenge, the presented work aims to assess the feasibility of laser

technology for joining thin sheets in a dissimilar configuration, specifically involving commercial

082-T6 sheet and stress-relieved AlSI10Mg sheets. The primary objective was to establish the

correlation between bead quality and energy consumption, with the goal of identifying the

optimal welding set-up that simultaneously optimizes these two crucial aspects. The effects of

filler wire, laser motion and welding parameters were studied in terms of both mechanical

properties and equivalent carbon emission consumption. The paper reports the optimal process

parameters that guarantee a weld bead with porosity less than 4% for all the configurations

tested, except for the case of linear laser motion without filler wire. This specific configuration

proved unsuitable and was consequently excluded from our final considerations. Concerning weld

bead quality, the employment of filler wire brings low aspect-ratio weld beads, particularly when

wobbling is activated. Wobbling induces larger widths because of its stirring effect on the melt

pool, resulting in an overall reduction in penetration depth. A similar effect was observed in joints

performed without filler wire, but the stirring effect of wobbling is less pronounced. In terms of

welding parameters and their impact on weld quality, increasing the welding speed and/or

lowering laser power reduces both the size and quantity of pores. With this general trend

established, the tested process conditions showed that joints with porosity below 4% can be

achieved, and optimized parameters facilitate a reduction in porosity to below 2%. Notably, the

two contrasting conditions - "wire with wobbling" (Group D) and "direct and linear" (Group A)-

exhibit a broader process operating window for Class B joints, as illustrated in Figure 4. Samples

from Group D are characterized by a high resistivity. Tensile-shear tests resulted in the highest

failure load (5.9 kN ± 0.37) and equivalent US (204 MPa ± 9.8). Second for the highest failure load

value are the welds in group A with 5.3 kN, exhibiting a failure load of 19 MPa. Slightly lower

mechanical strength was registered for optimized Group B samples, with a failure load and

ultimate strength of 4.8 kN and 191 MPa, respectively. Group A configuration proves to be very

interesting from a sustainable process perspective. The carbon emissions for the mentioned welding setups were computed utilizing the data from Tables 6 and 7, employing the approach and assumptions outlined earlier, and have undergone cross-verification. Taking into account the optimal process parameters for each group, the measured and estimated total carbon emissions per unit of welding length are as follows: 45.4 gCO2eq/m for Group A, 94.8 gCO2eq/m for Group B, and 108.9 gCO2eq/m for Group D. The absence of filler material, coupled with the lowest power (2 kW) and the highest speed (35 mm/s) that optimized this welding condition, contributes to a low CEeq consumption for Group A. The CEeq difference between optimized Group A and D is 140 %. This disparity is mainly attributed to emissions related to wire material production (66.7%) estimated by α_w coefficient (Table 3). It is followed by the impact of scanning speed which ranges from 25 to 35 mm/s (20.6 %) and finally by a decrease in laser power from 2.2 to 2 kW (~ 6%). In this scenario, Figure 9 compares the estimated carbon emissions of each subsystem. The primary contributor of carbon emissions is electricity consumption, with a significant impact from the laser beam generation system, followed by energy consumption in the cooling system. The motion systems, both related to laser motion and wire feeder, make a minimal contribution due to the relatively light load on the robot arm, and the low energy requirements for the wire feeder system. Other emission costs are related to the material consumption, both in terms of compressed gas and filler wire. Groups B and D make use of filler material, which represents one of the most cost-effective factors in terms of emissions. The other non-operative addendums become significant when the integrated industrial scenario is characterized by low productivity and fast processing of components (i.e., shorter welding length). Hence, reducing the standby time of the system also improves the carbon emission performance.

Productivity assumes a significant role when maximum quality or maximum sustainability requirements are no longer sufficient to identify a preferable welding condition. Paragraph 3.3 has indeed highlighted that the relationship between process time and standby time (or non-operational time) allows for identifying industrial scenarios where the choice of the best welding process varies. More specifically, in scenarios where high productivity is in demand, the combination of linear movement and no filler wire makes welding condition A a preferable option, allowing a faster process and large CO_2 emission savings.

On the other hand, the impact of CO_2 emissions decreases as the weight of processing time drops in the ratio of process time to standby time. This leads the choice towards a set up (Group D) that ensures better quality without significant environmental impact disadvantages.

5. CONCLUSION

This study investigates laser welding of dissimilar aluminum alloy sheets using linear scanning and laser beam wobbling, both with and without filler wire. Different process parameters are tested for various configurations, with the main aim of identifying the optimal welding configuration that achieves the required strength, minimal defects, suitable morphology, and low equivalent carbon emissions.

Defects, such as porosity < 2%, are minimized with filler wire, employing both linear and wobbled scanning strategies, as well as without wire and linear motion. The optimal process parameters were identified for each of these scenarios; however, when considering the strength and environmental sustainability criteria, the opposite "wire and wobbling" and "no wire and linear" scenarios are the most interesting. Specifically, laser power and welding speed required for high-quality welding were 2200 W and 25 mm/s in the "wire and wobbling" configuration and 2000 W and 35 mm/s in the "no wire and linear" configuration, highlighting the beneficial effect of linear

motion on productivity. On the other hand, porosity determined the highest joint strength when welded in a "wire and wobbling" configuration. The emission analysis results indicate that the use of filler wire leads to a significant increase in carbon emissions, with a more significant effect than that due to direct power consumption. The welding speed is the process parameter that has the biggest impact, which is the dominant factor that influences the carbon efficiency of the laser welding system because the gradient of welding speed is greater than that of laser power. The faster the welding speed is, the higher the carbon efficiency the laser welding system will reach. In conclusion, laser welding with filler wire and wobbling motion enables joining in a broad process window, achieving the highest mechanical properties; however, linear welding may also be a preferable option for achieving high productivity and low environmental impact.

REFERENCES

[1] IEA, Global CO2 emissions from energy combustion and industrial processes, 1900-2022, IEA, Paris [WWW Document], n.d., https://www.iea.org/data-and-statistics/charts/global-co2-emissions-from-energy-combustion-and-industrial-processes-1900-2022.

[2] I.E Agency (2023) world energy Outlook 2023 [Online] [WWW Document], n.d. . https://iea.blob.core.windows.net/assets/66b8f989-971c-4a8d-82b0-4735834de594/WorldEnergyOutlook2023.pdf.

[3] Chen, Q., Lai, X., Gu, H., Tang, X., Gao, F., Han, X., Zheng, Y., 2022. Investigating carbon footprint and carbon reduction potential using a cradle-to-cradle LCA approach on lithium-ion batteries for electric vehicles in China. Journal of Cleaner Production 369, 133342. https://doi.org/10.1016/j.jclepro.2022.133342

[4] Goffin, N., Jones, L.C.R., Tyrer, J., Ouyang, J., Mativenga, P., Woolley, E., 2021. Mathematical modelling for energy efficiency improvement in laser welding. Journal of Cleaner Production 322, 129012. https://doi.org/10.1016/j.jclepro.2021.129012

[5] Capello, E., 2008. Le lavorazioni industriali mediante laser di potenza.

[6] Cao, X., Jahazi, M., Immarigeon, J.P., Wallace, W., 2006. A review of laser welding techniques for magnesium alloys. Journal of Materials Processing Technology 171, 188–204. https://doi.org/10.1016/j.jmatprotec.2005.06.068

[7] Liverani, E., Ascari, A., Fortunato, A., 2023. The role of filler wire and scanning strategy in laser welding of difficult-to-weld aluminum alloys. The International Journal of Advanced Manufacturing Technology 128, 763-777. https://doi.org/10.1007/s00170-023-11932-x

[8] Saariluoma, H., Piiroinen, A., Unt, A., Hakanen, J., Rautava, T., Salminen, A., 2020. Overview of Optical Digital Measuring Challenges and Technologies in Laser Welded Components in EV Battery Module Design and Manufacturing. Batteries 6, 47. https://doi.org/10.3390/batteries6030047

[9] ISO 14044:2006-environmental management—life cycle assessment—requirements and guidelines (2006)

[10] Yilbas, B. S., Shaukat, M. M., Afzal, A. A., Ashraf, F., 2020. Life cycle analysis for laser welding of alloys. Optics & Laser Technology 126, 106064. https://doi.org/10.1016/j.optlastec.2020.106064.

[11] Sproesser, G., Chang, Y. J., Pittner, A., Finkbeiner, M., Rethmeier, M., 2015. Life Cycle Assessment of welding technologies for thick metal plate welds, Journal of Cleaner Production 108, 46-53. https://doi.org/10.1016/j.jclepro.2015.06.121.

[12] Sangwan, K.S., Herrmann, C., Egede, P., Bhakar, V., Singer, J., 2016. Life Cycle Assessment of Arc Welding and Gas Welding Processes. Procedia CIRP 48, 62-67. https://doi.org/10.1016/j.procir.2016.03.096.

[13] Xydea, E., Panagiotopoulou, V.C., Stavropoulos, P., 2024. A strategy framework for identifying carbon intensive elements in welding processes. Procedia CIRP 121, 103-108, https://doi.org/10.1016/j.procir.2023.09.236.

[14] Wei, H., Zhang, Y., Tan, L., Zhong, Z., 15 January 2015. Energy efficiency evaluation of hot-wire laser welding based on process characteristic and power consumption. J. Clean. Prod. 87, 255e262. http://dx.doi.org/10.1016/j.jclepro.2014.10.009.

[15] Feng, S., Senthilkumaran, K., Brown, C., Kulvatunyou, B., 2014. Energy metrics for product assembly equipment and processes, Journal of Cleaner Production 65, 142-151. http://dx.doi.org/10.1016/j.jclepro.2013.09.044

[16] Ge, W., Li, H., Cao, H., Li, C., Wen, X., Zhang, C., Mativenga, P., 2023. Welding parameters and sequences integrated decision-making considering carbon emission and processing time for multi-characteristic laser welding cell. Journal of Manufacturing Systems 70, 1-17. https://doi.org/10.1016/j.jmsy.2023.07.001.

[17] Ge, W., Cao, H., Li, H., Zhang, C., Li, C., Wen, X., 2022 Multi-feature driven carbon emission time series coupling model for laser welding system. Journal of Manufacturing Systems 65, 767-784. https://doi.org/10.1016/j.jmsy.2022.11.005.

[18] Wu, J., Zhang, C., Giam, A., Chia, H. Y., Cao, H., Ge, W., Yan, W., 2024. Physics-assisted transfer learning metamodels to predict bead geometry and carbon emission in laser butt welding. Applied Energy, 359, 122682. https://doi.org/10.1016/j.apenergy.2024.122682.

[19] Chen, C., Liu, Y., Kumar, M., Qin, J., Ren, Y., 2019. Energy consumption modelling using deep learning embedded semi-supervised learning. Computers & Industrial Engineering 135, 757–765. https://doi.org/10.1016/j.cie.2019.06.052

[20] Li, J., Cao, L., Hu, J., Sheng, M., Zhou, Q., Jin, P., 2022. A prediction approach of SLM based on the ensemble of metamodels considering material efficiency, energy consumption, and tensile strength. J Intell Manuf 33, 687–702. https://doi.org/10.1007/s10845-020-01665-z

[21] Wu, J., Zhang, C., Lian, K., Cao, H., Li, C., 2022. Carbon emission modeling and mechanical properties of laser, arc and laser–arc hybrid welded aluminum alloy joints. Journal of Cleaner Production 378, 134437. https://doi.org/10.1016/j.jclepro.2022.134437

[22] Yan, W., Zhang, H., Jiang, Z., Hon, K.K.B., 2017. Multi-objective optimization of arc welding parameters: the trade-offs between energy and thermal efficiency. Journal of Cleaner Production 140, 1842–1849. https://doi.org/10.1016/j.jclepro.2016.03.171

[23] Peng, S., Li, T., Zhao, J., Lv, S., Tan, G.Z., Dong, M., Zhang, H., 2019. Towards energy and material efficient laser cladding process: Modeling and optimization using a hybrid TS-GEP algorithm and the NSGA-II. Journal of Cleaner Production 227, 58–69. https://doi.org/10.1016/j.jclepro.2019.04.187

[24] Zhang, C., Zhou, Z., Tian, G., Xie, Y., Lin, W., Huang, Z., 2018. Energy consumption modeling and prediction of the milling process: A multistage perspective. Proceedings of the Institution of Mechanical Engineers, Part B: Journal of Engineering Manufacture 232, 1973–1985. https://doi.org/10.1177/0954405416682278

[25] Huang, Z., Cao, H., Zeng, D., Ge, W., Duan, C., 2021. A carbon efficiency approach for laser welding environmental performance assessment and the process parameters decision-making. Int J Adv Manuf Technol 114, 2433–2446. https://doi.org/10.1007/s00170-021-07011-8

[26] Sun, T., Franciosa, P., Sokolov, M., Ceglarek, D., 2020. Challenges and opportunities in laser welding of 6xxx high strength aluminium extrusions in automotive battery tray construction. Procedia CIRP 94, 565–570. 10.1016/j.procir.2020.09.076

[27] https://www.ipgphotonics.com/en

[28] Daintith, J., 2009. A dictionary of physics, 6th ed. ed. Oxford University Press, Oxford.

[29] Ferrari, E., 2021. Servizi generali di impianto. Società Editrice Esculapio.

[30] Wang, G.G., Shan, S., 2007. Review of Metamodeling Techniques in Support of Engineering Design Optimization. Journal of Mechanical Design 129, 370–380. https://doi.org/10.1115/1.2429697

[31] Bastos, J., Lo Vullo, E., Muntean, M., Duerr, M., Kona, A., Bertoldi, P., 2020. GHG Emission Factors for Electricity Consumption. European Commission, Joint Research Centre (JRC) [Dataset] PID: http://data.europa.eu/89h/919df040-0252-4e4e-ad82-c054896e1641

[32] Janjua, R., Maciel, F., 2023. CO2 Data Collection, Review 2022. World Steel Association

[33] International Aluminium Institute (IAI), 2023. Greenhouse Gas Emissions Intensity- Primary Aluminium, reference period: 2022. n.d., https://international-aluminium.org/statistics/greenhouse-gas-emissions-intensity-primary-aluminium

FIGURE CAPTION

Figure 2: Methodology adopted for the laser welding process optimization following quality and sustainability criteria.

Figure 2: Signal acquisition and processing method for the evaluation of $CO_{2,eq}$ emissions.

Figure 3: Priority of the selection criteria as the requirements and industrial scenario change.

Figure 4: Frequency of sample identification based on porosity class in the four analyzed process conditions (Groups A, B, C, D).

Figure 5: Lower-class porosity weald beads for each condition: group A) 2 kW, 35 mm/s; B) 2.2 kW, 35 mm/s; C) 2 kW, 25 mm/s; D) 2.2 kW, 25 mm/s.

Figure 6: Results of tensile-shear tests in terms of Equivalent Ultimate Strength.

Figure 7. Equivalent carbon emissions for different process parameters in welding without filler wire.

Figure 8. Influence of laser speed and power when welding without filler wire. Welding speed exerts the most significant influence.

Figure 9. Equivalent carbon emissions for various process parameters in welding with filler wire.

Figure 10. Influence of factors involved in calculating equivalent carbon emission of the optimized welding conditions. The use of filler wire is ranked first, with an increase of 109% for Group B and of 140% for Group D, followed by laser speed, which shows a +28% increase in Group C.

Figure 11. Contribution of CE in operational and standby phases

Figure 12. Influence of laser speed and weld length when welding with filler wire. The weld length is the variable that exerts the most significant influence.

Figure 13. Analysis of the trade-off in the choice of welding condition.

Figure 14. Final definition of priority in the selection criteria.

Table 7: Characteristics of laser equipment.

Table 8: Welding process parameters divided into four categories: welding without filler wire and linear motion (Group A), welding with filler wire and linear motion (Group B), welding without filler wire and wobbling (Group C) and welding with filler wire and wobbling (Group D).

Table 9. Relevant coefficients of carbon emission

Table 10: Welding process parameters selected for tensile-shear tests.

Table 11. Active powers measured during welding process.

Table 12. Carbon emissions calculations for various parameters in welding without filler wire.

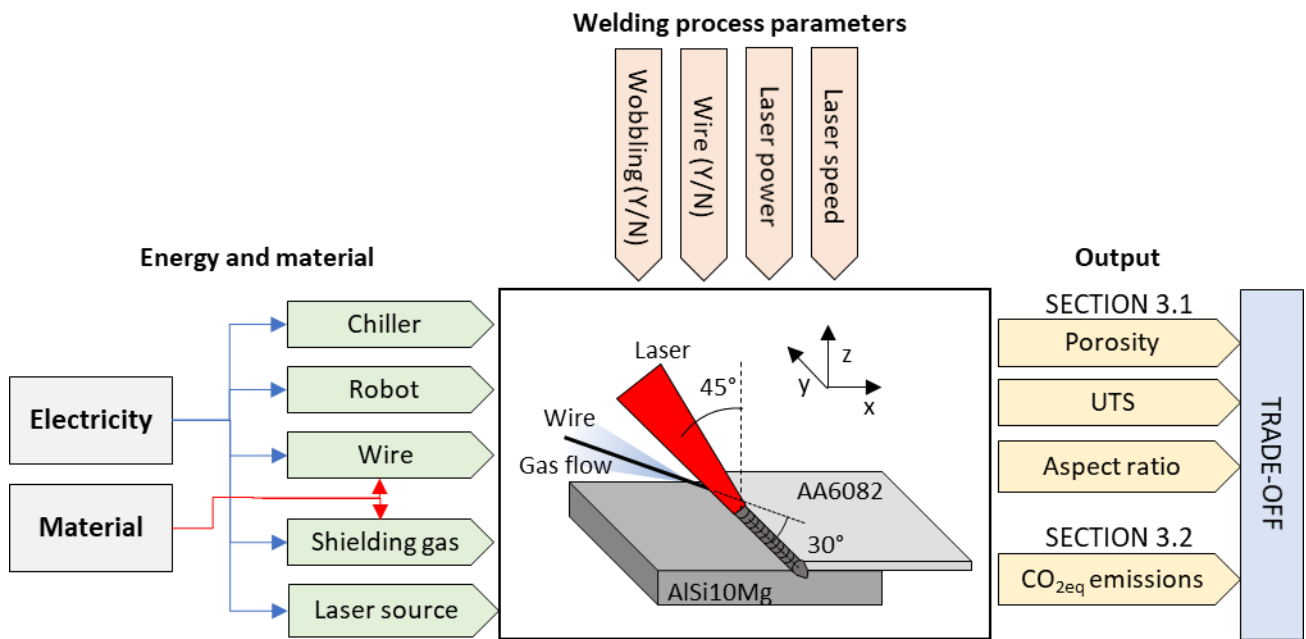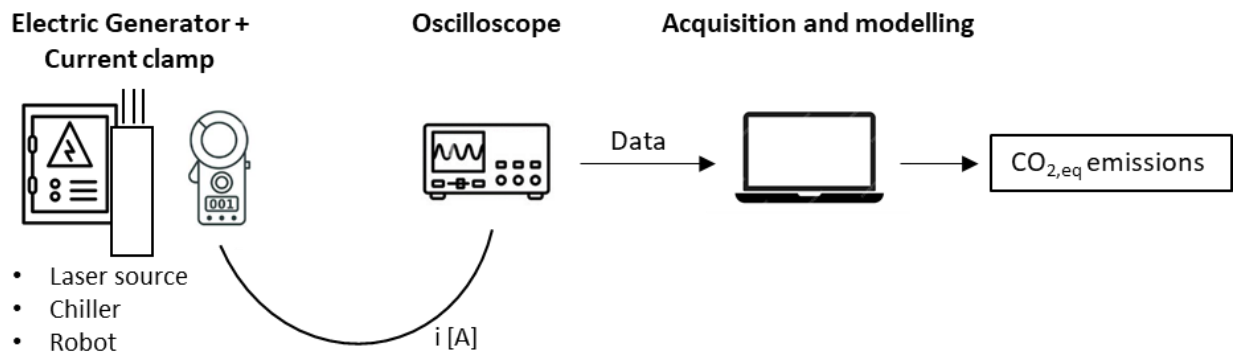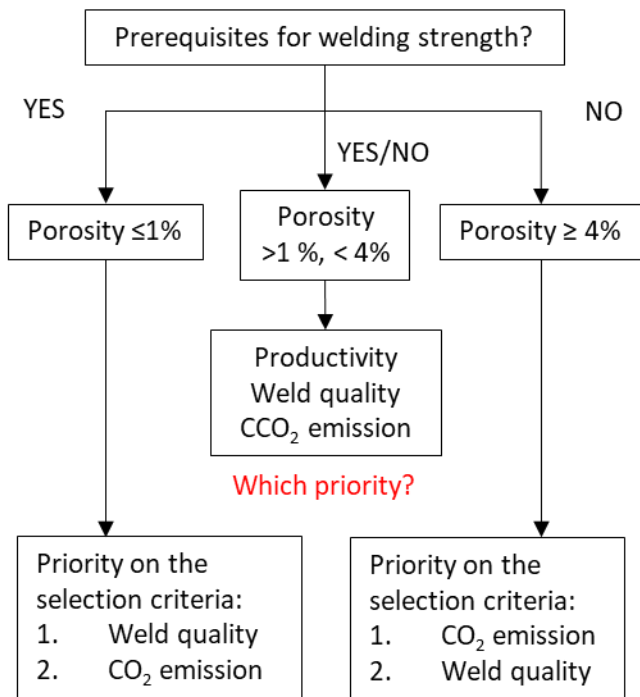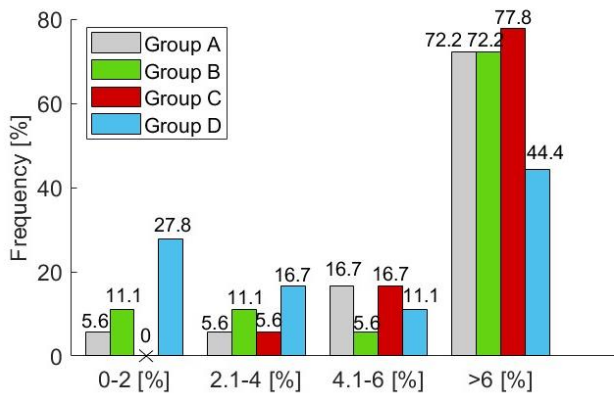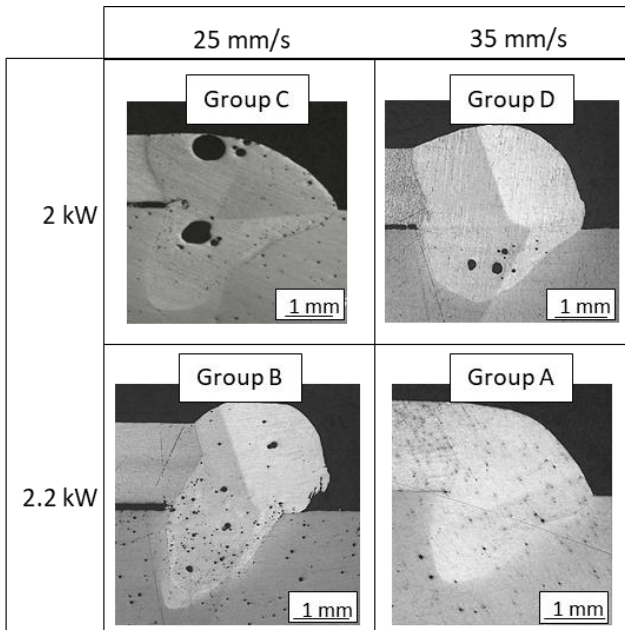Table 7. Carbon emissions calculations for various parameters in welding with filler wire.
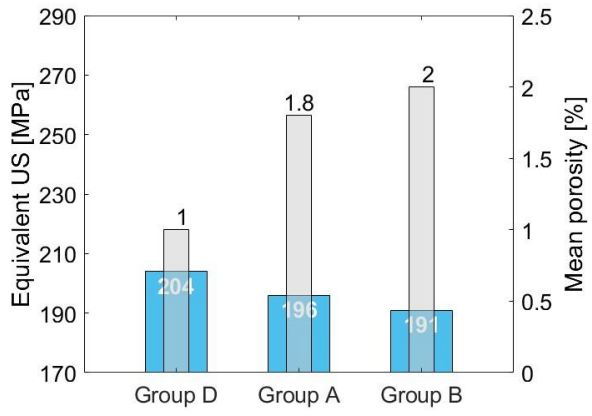
Figure 3
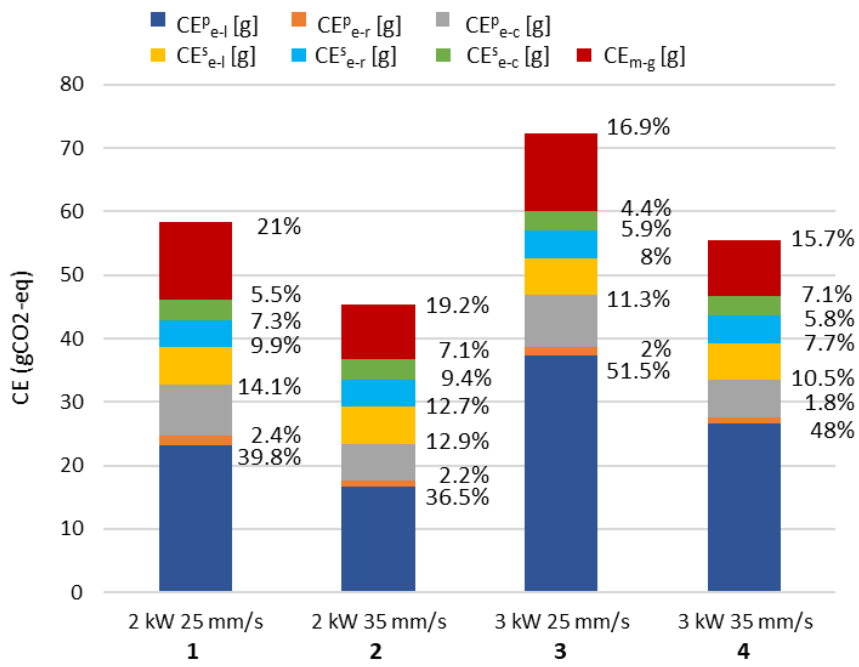
Figure 2

Figure 3

Figure 4

Figure 5

Figure 6

Figure 7
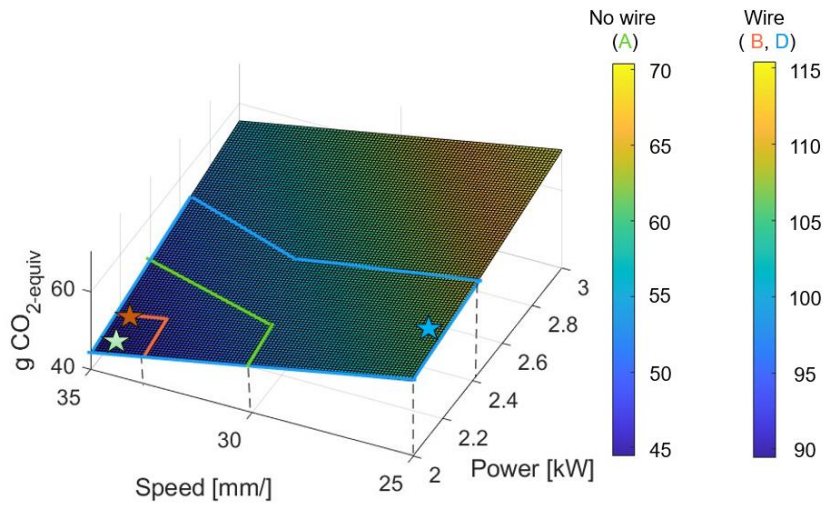
Figure 8

Figure 9

Figure 10

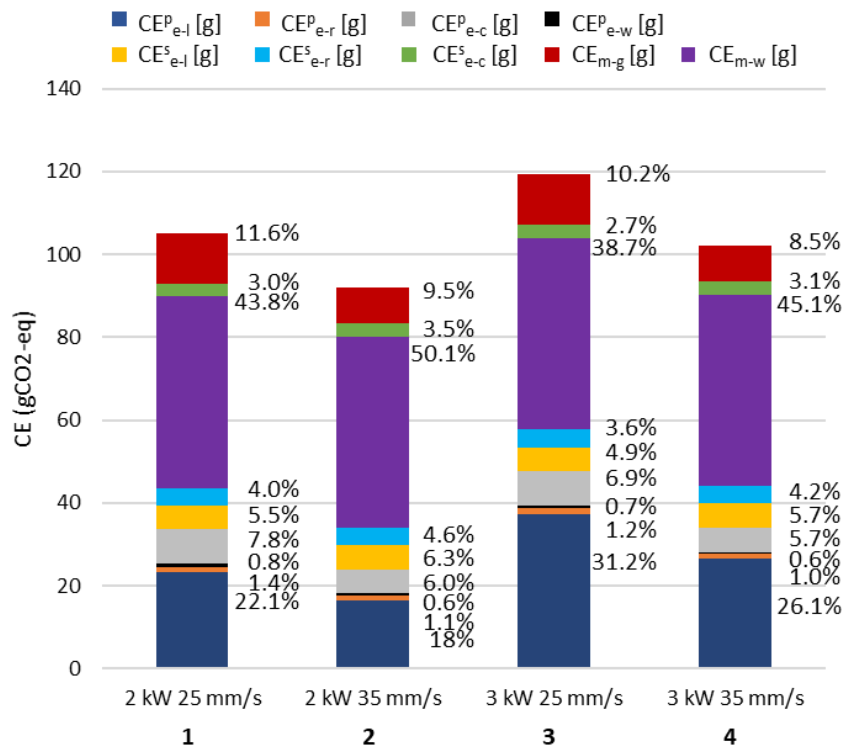| Optimized A	Optimized D
WL: 1m; t_s:60 s	WL: 1m; t_s:60 s
(a)	(b)
WL: 0.1m; t_s:60 s	WL: 0.1m; t_s:60 s
(c)	(d)
WL: 1m; t_s:60 s	WL: 1m; t_s:60 s
(e)	(f)

Legend: CE^s (green), CE^p (orange)
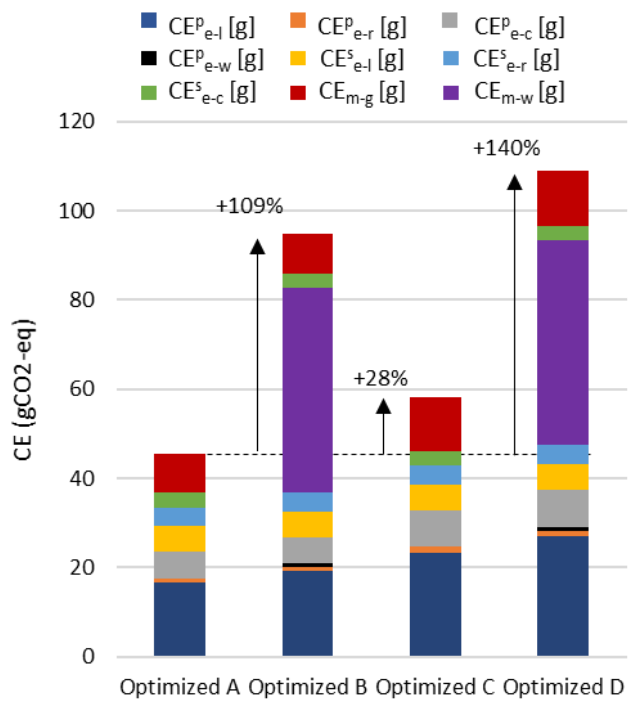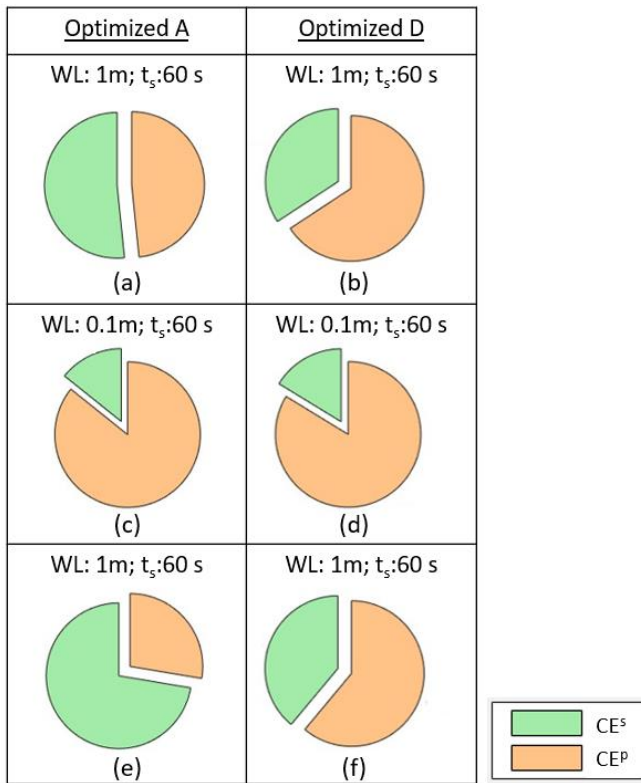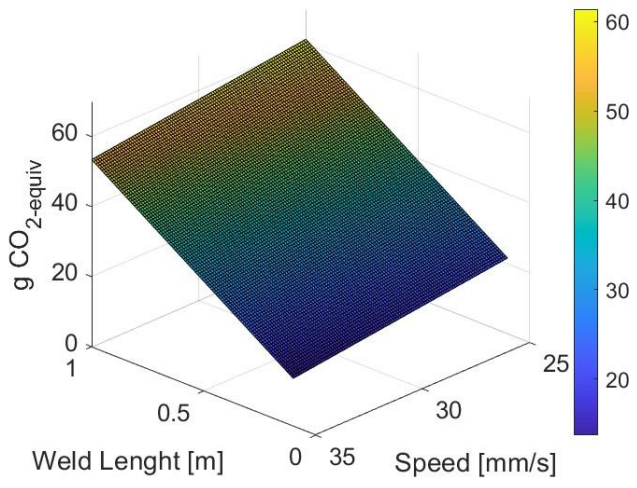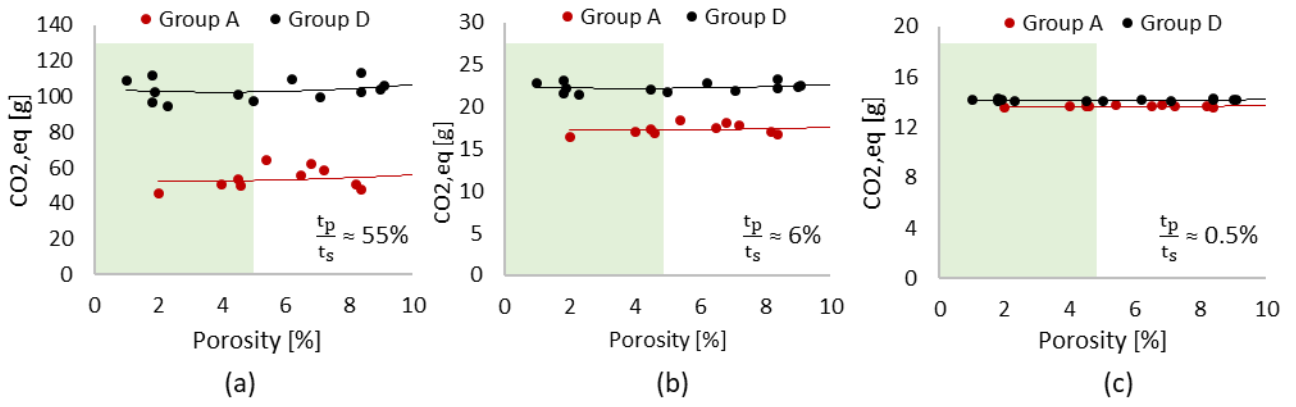
Figure 11

Figure 12

Figure 13.
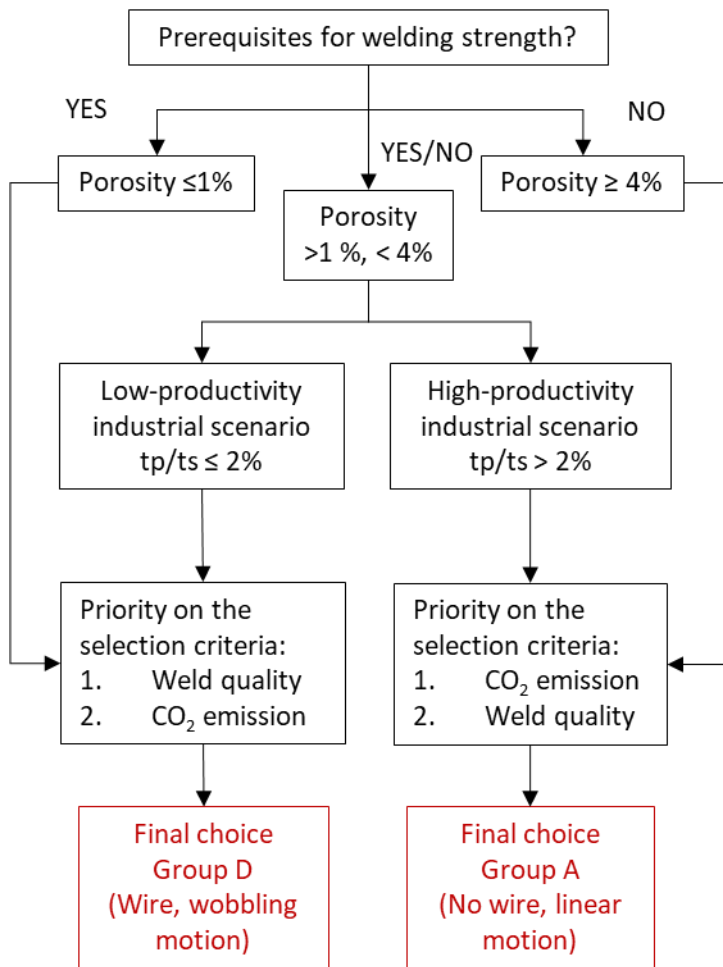
Figure 14.

Table 13

Maximum Power	6 kW
BPP	4 mm·
Collimation focal length	200 mm
Focalization focal length	300 mm
Magnification factor	1.5
Fiber core diameter	100 µm
Spot diameter	150 µm
Maximum wobbling frequency	350 Hz

Table 14

Test	Wobbling	Filler Wire	Laser power [kW]	Welding speed [mm/s]	Wire speed [m/min]
A (1-18)	N	N			/
B (1-18)	N	Y	2-3 every 0.2	25; 30; 35	1.5; 1.8; 2.1
C (1-18)	Y	N			/
D (1-18)	Y	Y			1.5; 1.8; 2.1

Table 15

α_e	0.267 kgCO$_{2eq}$/kWh	[31]
α_{gas}	0.611 kgCO$_{2eq}$/m^3	[32]
α_w	15.1 kgCO$_{2eq}$/kg	[33]

Table 16

Group	Wobbling	Filler Wire	Laser power [kW]	Welding speed [mm/s]	Wire speed [m/min]
A	N	N	2	35	/
B	N	Y	2.2	35	2.1
C	Y	N	2	25	/
D	Y	Y	2.2	25	1.5

Table 17

Welding Power [kW] Active power	2	2.2	2.4	2.6	2.8	3
P_l^p	7.82	9.06	9.89	10.41	11.30	12.56
P_c^p	2.76					
P_r^p	0.48					
P_w^p	0.28					
P_l^s	1.30					
P_c^s	0.72					
P_r^s	0.48					

Table 18.

P_l [kW]	v_l [mm/s]	CE^p_{e-l} [g]	CE^p_{e-r} [g]	CE^p_{e-c} [g]	CE^p_e [g]	CE^s_{e-l} [g]	CE^s_{e-r} [g]	CE^s_{e-c} [g]	CE_{m-g} [g]	CEeq [g]
2	25	23.20	1.42	8.19	32.81				12.22	57.29
	30	19.33	1.18	6.82	27.34				10.18	50.79
	35	16.57	1.02	5.85	23.44				8.73	45.43
2.2	25	26.88	1.42	8.19	36.49				12.22	61.97
	30	22.40	1.18	6.82	30.41				10.18	53.85
	35	19.20	1.02	5.85	26.06				8.73	48.05
2.4	25	29.34	1.42	8.19	38.95				12.22	64.43
	30	24.45	1.18	6.82	32.46				10.18	55.91
	35	20.96	1.02	5.85	27.82	5.79	4.27	3.20	8.73	49.81
2.6	25	30.88	1.42	8.19	40.50				12.22	65.98
	30	25.74	1.18	6.82	33.75				10.18	57.19
	35	22.06	1.02	5.85	28.93				8.73	50.92
2.8	25	33.52	1.42	8.19	43.14				12.22	68.62
	30	27.94	1.18	6.82	35.95				10.18	59.39
	35	23.95	1.02	5.85	30.81				8.73	52.80
3	25	37.26	1.42	8.19	46.87				12.22	72.35
	30	31.05	1.18	6.82	39.06				10.18	62.51
	35	26.62	1.02	5.85	33.48				8.73	55.47

Table 7

P_l [kW]	$v_l - v_f$ [mm/s - [m/min]	CE^p_{e-l} [g]	CE^p_{e-r} [g]	CE^p_{e-w} [g]	CE^p_{e-c} [g]	CE^s_{e-l} [g]	CE^s_{e-r} [g]	$CE_{m.w}$ [g]	CE^s_{e-c} [g]	$CE_{m.g}$ [g]	$CEeq$ [g]
2.0	25-1.5	23.20	1.42	0.82	8.19					12.22	105.22
	30-1.8	19.33	1.19	0.68	6.82					10.18	97.58
	35-2.1	16.57	1.02	0.58	5.85					8.73	92.12
2.2	25-1.5	26.88	1.42	0.82	8.19					12.22	108.90
	30-1.8	22.40	1.19	0.68	6.82					10.18	100.65
	35-2.1	19.20	1.02	0.58	5.85					8.73	94.75
2.4	25-1.5	29.34	1.42	0.82	8.19					12.22	111.36
	30-1.8	24.45	1.19	0.68	6.82					10.18	102.70
	35-2.1	20.96	1.02	0.58	5.85	5.79	4.27	46.11	3.20	8.73	96.51
2.6	25-1.5	30.88	1.42	0.82	8.19					12.22	112.91
	30-1.8	25.74	1.19	0.68	6.82					10.18	103.98
	35-2.1	22.06	1.02	0.58	5.85					8.73	97.61
2.8	25-1.5	33.52	1.42	0.82	8.19					12.22	115.55
	30-1.8	27.94	1.19	0.68	6.82					10.18	106.18
	35-2.1	23.95	1.02	0.58	5.85					8.73	99.50
3.0	25-1.5	37.26	1.42	0.82	8.19					12.22	119.28
	30-1.8	31.05	1.19	0.68	6.82					10.18	109.30
	35-2.1	26.62	1.02	0.58	5.85					8.73	102.17